Fluvial-aeolian interactions in sedimentary signal buffering: an example from the Indus Basin – Thar Desert

Amy E. East*

U.S. Geological Survey, 400 Natural Bridges Drive, Santa Cruz, CA 95060, USA

Peter D. Clift

Department of Geology and Geophysics, Louisiana State University, Baton Rouge LA 70803, USA

Andrew Carter

Department of Earth and Planetary Sciences, Birkbeck College, University of London, Malet Street, London WC1E 7HX, United Kingdom

Anwar Alizai

Geological Survey of Pakistan, ST-17/2, Gulistan-e-Jauhar, Karachi, Pakistan

Sam VanLaningham

Oregon State University, Cascades Campus, 2600 NW College Way, Bend OR 97701

*Corresponding author; aeast@usgs.gov; +1-831-460-7533

ABSTRACT

Sediment production and its subsequent preservation in the marine stratigraphic record offshore of large rivers are linked by complex sediment-transfer systems. To interpret this record it is critical to understand how environmental signals transfer from sedimentary source regions to depositional sinks, and in particular to understand the role of buffering in obscuring climatic or tectonic signals. In dryland regions, signal buffering can include sediment cycling through linked fluvial and aeolian systems. We investigate sedimentary coupling between the Indus River and the Thar Desert, where fluvial and aeolian systems have exchanged sediment over large spatial scales (100s km) since at least 6 ka. Summer monsoon winds recycle sediment from the lower Indus River and delta northeastward, i.e., downwind and upstream, into the desert. Far-field aeolian recycling of Indus sediment is important enough to control sediment provenance at the downwind end of the desert substantially, although the proportion of Indus sediment of various ages varies regionally within the desert; dune sands in the northwestern Thar Desert resemble the Late Holocene–Recent Indus delta, requiring short transport and reworking times. On smaller spatial scales (1–10 m) along fluvial channels in the Thar Desert, there is also stratigraphic evidence of fluvial and aeolian sediment reworking from local rivers. In terms of sediment volume, we estimate that the Thar Desert could be a more substantial sedimentary store than all other known buffer regions in the Indus basin combined. Thus, since the mid-Holocene, when the desert expanded as the summer monsoon rainfall decreased, fluvial-aeolian recycling has been an important but little recognized process

buffering sediment flux to the ocean. Similar fluvial-aeolian coupling likely also affects sedimentary signal transfer in other dryland regions globally.

Keywords: fluvial-eolian interaction; sediment transport; signal buffering; Thar; Indus

INTRODUCTION

During passage from source areas to long-term depositional sinks, a fraction of the sediment in transport in a river is extracted and stored at least temporarily, resulting in net sediment loss from the transfer system (e.g., Trimble et al. 1983; Dunne et al. 1998; Petter et al. 2013). Stored sediment is later released and mixed with new river sediment to generate a potentially complicated sedimentary signal in the depocenter, especially in large drainage basins. In this manner, erosional pulses caused by climatic change or tectonic events may be 'buffered', and any signals resulting from changes in sediment flux may be diffused or entirely obscured in the downstream sedimentary record. The transmission of sediment-flux signals is a function of (1) transport efficiency within the sediment-transfer system, and (2) sediment extraction (long-term sequestration of sediment in a net-aggradational system).

The efficiency with which rivers transfer and export sediment depends upon the relationship between sediment supply and a landscape system's ability to export sediment. Alluvial rivers, in particular, limit the efficiency of watershed sediment export, buffering the transmission of environmental signals by storing sediment in overbank and floodplain deposits (Castelltort and Van den Driessche 2003; Simpson and Castelltort 2012;

69 Armitage et al. 2013; Pizzuto 2014). As a result, environmental perturbations on shorter
70 time scales than the time needed for downstream signal propagation may not be evident
71 in the stratigraphic record of the ultimate depositional sink. The longer the transport
72 pathway of an alluvial system, the less effectively it may transmit short-lived
73 environmental signals, resulting in a greater buffering effect (Castelltort and Van den
74 Driessche, 2003).

75 Signal buffering has been most intensively studied and modeled for alluvial rivers,
76 but is less well understood in other sedimentary systems. Accommodation space on low-
77 gradient coastal plains, deltas, and continental shelves can impart additional buffering
78 effects, though without necessarily erasing all short-term climatic signals from the
79 downstream stratigraphic record (Goodbred 2003; Clift et al. 2008; Wolinsky et al. 2010;
80 Forzoni et al. 2014). Quaternary valley fill and mass-wasting deposits near mountainous
81 source areas can be important sediment stores as well (Blöthe and Korup 2013; Clift and
82 Giosan 2014). Notably, in dryland (arid and semi-arid) regions sediment routing includes
83 seldom-studied interactions between fluvial and aeolian processes that are likely to
84 introduce additional complexity (e.g., Bullard and Livingstone 2002; Belnap et al. 2011).

85 Aeolian deposits are both sources and sinks of fluvial sediment in arid and semi-
86 arid lands (e.g., Ramsey et al. 1999; Bullard and Livingstone 2002; Prins et al. 2009;
87 Roskin et al. 2014). Fluvially sourced aeolian dunes form as the wind reworks fluvial
88 sediment into source-bordering dunes along the river margin that can feed dune fields
89 progressively farther downwind of the river (Bullard and McTainsh 2003; Han et al.
90 2007; Gibling et al. 2008; Amit et al. 2011; Draut 2012). Wind can carry sediment 100s
91 of km downwind from river channels, deltas, and from continental shelf deposits exposed

during low sea level (Muhs et al. 2003; Amit et al. 2011), in some cases moving sediment back toward its source area. As a result, large dune fields such as the Thar Desert (India and Pakistan; Fig. 1A) have substantial potential for buffering sediment movement from source areas toward the ocean.

Despite their potential to disrupt source-to-sink transport, links between fluvial and aeolian processes are not widely recognized as interrupting environmental signal transfer. This study synthesizes new and previously published stratigraphic and sediment-provenance data, and quantifies provenance relations between Thar Desert sand samples and fluvial sediment up- and downwind, to evaluate recycling of sand between the Indus River and the Thar Desert over Holocene time. We infer that fluvial-aeolian sediment recycling likely constitutes a major buffer, with the desert being probably the largest storage zone in the Indus sediment-routing system. We propose that similar fluvial-aeolian connectivity probably affects signal transfer in other dryland regions, but that its importance has been little recognized.

REGIONAL SETTING AND PREVIOUS WORK

The Indus River is the only major river draining the western Himalaya and Karakoram ranges (Fig. 1). It delivers sediment to the Arabian Sea, building the world's second-largest submarine fan. The Indus has a long history of drainage evolution, including, in Holocene time, abandonment of the Yamuna River course in the northeastern Punjabi floodplain owing to headwater capture (Valdiya 2002; Saini et al. 2009; Clift et al. 2012) and the drying up of the Ghaggar-Hakra River tributary after ~4 ka (Giosan et al. 2012). Fluvial sediment recycling in the Indus system is apparent from

115 incision of rivers into northern half of the floodplains, adjacent to the Himalaya (whereas
116 the southern portion of the floodplain adjacent to the delta continues to aggrade); Clift
117 and Giosan (2014) estimated that incision and reworking of sediment from the northern
118 floodplains accounts for 21–23% of the flux into the coastal zone since the LGM, totaling
119 >900 km^3. There has been incision of river valleys into the northern parts of the Punjabi
120 floodplains at the northern (downwind) side of the Thar Desert since the early Holocene
121 (Giosan et al. 2012), reworking sediment 10 ka and older. Sediment sequestration in
122 Himalayan valley fill and mass-wasting deposits also introduces additional sediment
123 residence times of 1–100 kyr in some regions of the Indus and Ganges-Brahmaputra
124 River systems (Blöthe and Korup 2013).
125 The Thar Desert dates from at least Mid-Pleistocene time (Wasson et al. 1983;
126 Glennie et al. 2002; Singhvi et al. 2010). The southwest summer monsoon is the
127 prevailing influence on wind and rainfall in this region, with aeolian sediment transport
128 dominantly from southwest toward northeast (Fig. 1); summer months typically include
129 dry, windy conditions, commonly with dust storms, followed by late summer rain
130 (Singhvi et al., 2010). Winter winds play a substantially lesser role in sand transport and
131 dune formation, and their principal effects are restricted to the northern Thar Desert (Kar,
132 1993). The desert is bounded to the west by the Indus River and its eastern tributaries,
133 including the Sutlej River immediately to the north.
134 Several studies have described and dated sedimentary profiles from the Thar
135 Desert and neighboring fluvial environments, revealing the timing of sediment storage
136 and erosion. These show that the Thar Desert expanded after the LGM, during phases of
137 strengthened summer monsoon (Singhvi et al., 2010). However, the desert also continued

its advance westward during weakening of the summer monsoon starting after ~8 ka (e.g., Gupta et al. 2003). A ~200-kyr record from the east-central Thar Desert of sediment composition, mineralogy, and optically stimulated luminescence (OSL) and thermoluminescence (TL) ages showed at least 12 cycles of aeolian sedimentation, alternating with geomorphic stability accompanied by soil formation (Singhvi et al. 2010). Several sedimentary profiles with relevance for dating desert evolution and determining provenance are reproduced in Figure 2 (Singhvi and Kar 2004; Clift et al. 2008; Alizai et al. 2011a; Giosan et al. 2012), demonstrating the westward expansion of the desert during Holocene time. Singhvi and Kar (2004) inferred rapid sediment accumulation in the central part of the desert through the Holocene—for example, 7 m of accretion since the LGM at Chamu (Fig. 2). On the western edge of the desert, e.g., in the Nara Valley, the dunes have advanced over the floodplains more recently. Dunes yield ages ranging from ~1.42 ka at Yazman to 0.44 ka at Section MGJ-5, on the desert's northern side (Giosan et al. 2012; Fig. 2). In other locations the age of dune advance is interpreted to be necessarily younger than the underlying fluvial sediments, with the general trend indicating desert expansion after 4.8 ka (Durcan et al. 2010), during a phase of weakening monsoon rainfall (Enzel et al. 1999; Fleitmann et al. 2003; Gupta et al. 2003). At Chundkho, in the Nara region (Fig. 2), silty loess deposits also indicate dry, windy conditions between 4.8 and 7.0 ka, followed by burial of the loess by the expanding sand dune fields after 4.8 ka.

Connectivity between fluvial and aeolian sedimentary systems in the Indus watershed and Thar Desert—with the desert acting as both source and sink for fluvial material—has been documented to varying degrees by the aforementioned stratigraphic

studies and some provenance analyses. Earlier stratigraphic studies demonstrated local fluvial-aeolian coupling of dune sediment and fluvial material in the Thar Desert, river channels, and floodplains (Singhvi and Kar 2004; Clift et al. 2012; Giosan et al. 2012; Fig. 2). Fluvial erosion of aeolian dunes along the Nara River valley (likely a former south-flowing course or distributary of the Indus River), as well as along the former course of the Ghaggar-Hakra River, is clear from satellite images (Figs. 1B, C). That the Indus delta region serves as a sediment source for the Thar Desert is evident from foraminifera tests in the central and northeastern Thar Desert sand that are derived from shallow marine regions (Kameswara Rao et al., 1989). The importance of Thar Desert sediment sources originating in the lower Indus River and delta is also apparent from the dominant orientations of aeolian dunes throughout the desert—transverse, parabolic, and linear forms indicate the prevalence of north-northeastward aeolian sediment transport (Figs. 1A, 1C).

Initial sediment-provenance analyses have supported the concept that aeolian recycling of fluvial sediment could be a major influence in Indus sediment routing. As part of a study of Indus-basin drainage evolution since the Pleistocene, Alizai et al. (2011a, 2011b) demonstrated that Pb isotopes from detrital K-feldspar grains, as well as then-available U-Pb zircon and Nd isotopic data, showed similarity between the lower reaches of the mainstem Indus River (i.e., downstream of the last major tributary confluence) and the downwind (northern) Thar Desert. Here, we expand substantially upon previous provenance analyses by presenting new U-Pb zircon and Nd isotopic data from the Thar Desert and Indus basin. We use the new and previously existing data together to quantify provenance relations among the fluvial and aeolian components of

184 the Thar-Indus system. We use the resulting provenance relations to evaluate how
185 substantially fluvial-aeolian interactions over large spatial scales may have buffered
186 sediment delivery from the Indus River system to the ocean.
187
188 **PROVENANCE ANALYSIS: DATA SOURCES AND METHODS**
189 In order to assess the importance of various possible sediment sources
190 contributing to aeolian sand in the Thar Desert, and thus the importance of aeolian supply
191 from the lower Indus River and delta, we compiled available U-Pb zircon and Nd-isotope
192 provenance data from Thar Desert samples and surrounding fluvial environments. The
193 latter include the lower Indus River and delta spanning the time since the LGM, the Nara
194 Valley, and the southern part of the Punjabi floodplains (Sutlej River and downstream
195 end of the former Ghaggar-Hakra River course, which border the Thar Desert on the
196 downwind side; Fig. 1).
197 In addition to three new U-Pb zircon age spectra described below, we refer to the
198 U-Pb zircon provenance work of Clift et al. (2004, 2008) and Alizai et al. (2011a, b),
199 utilizing age spectra from: (1) an aeolian dune sand sample at site Chak-310 (Alizai et al.,
200 2011b); (2) a sample of modern fluvial sand from the Sutlej River at Tatapani close to
201 where this river leaves the Himalayan source area, in the downstream-most mountainous
202 terrain of the Sutlej basin (Alizai et al. 2011a; location in Fig. 1A); (3) a fluvial sediment
203 sample from a depth of 118 m in a borehole on the Indus delta at Keti Bundar dated to the
204 LGM (age loosely constrained to between 20 and 28.7 ka; Clift et al., 2008); (4) an Indus
205 River fluvial sand sample from a depth of 30 m in a borehole at Thatta (sample TH-10),
206 dated to 7 ka (Clift et al. 2008); and (5) a sample of modern lower Indus River fluvial

207 sand collected in the active river channel 200 m away from the Thatta borehole site (Clift
208 et al. 2004).

209 Samples of aeolian dune sand were collected for U-Pb detrital-zircon analysis
210 from two locations near the upwind, southern extent of the Thar Desert: UN1 and NM3
211 (Fig. 1A). We also analyzed the U-Pb zircon age spectrum from a fluvial sand sample
212 collected at a depth of 15 m in a borehole in the Nara Valley (Nara-1 drill site, Fig. 1C)
213 from which the full sedimentary profile (Fig. 2) was described by Alizai et al. (2011b)
214 and Giosan et al. (2012). Zircon grains were extracted from each of these three samples
215 and their U-Pb age spectra were determined from polished grain mounts by laser ablation
216 inductively coupled plasma mass spectrometry (LA-ICP-MS) at University College
217 London. This facility employs a New Wave 193 nm aperture-imaged, frequency-
218 quintupled laser ablation system coupled to an Agilent 7700 quadrupole-based ICP-MS.
219 The laser was set up to produce an energy density of ca 2.5 J/cm^2 at a repetition rate of 10
220 Hz. Repeated measurements of external zircon standard PLESOVIC (TIMS reference age
221 337.13±0.37 Ma; Sláma et al. 2008) and NIST 612 silicate glass (Pearce et al. 1997) were
222 used to correct for instrumental mass bias and depth-dependent inter-element
223 fractionation of Pb, Th and U. Temora (Black et al. 2003) and 91500 (Wiedenbeck et al.
224 2004) zircon were used as secondary age standards. Data were filtered using standard
225 discordance tests with a 15% cutoff. The $^{206}Pb/^{238}U$ ratio was used to determine ages
226 where < 1000 Ma, and the $^{207}Pb/^{206}Pb$ ratio for older grains. Data were processed using
227 GLITTER 4.4 data reduction software. Time-resolved signals that record evolving
228 isotopic ratios with depth in each crystal enabled filtering to remove spurious signals
229 owing to overgrowth boundaries, inclusions, or fractures. Data were then filtered using

230 standard discordance tests and applying a 10% cutoff. Between 96 and 186 grain ages
231 were measured in each sample, in order to generate a statistically meaningful data set
232 (Vermeesch 2004).

233 We compiled new and previously published analyses to examine Nd isotopic
234 provenance affinity as well, because this isotopic system is known to be resistant to the
235 effects of chemical weathering and has a proven record as a source discriminant in the
236 Indus basin (Clift et al. 2008, 2012). Furthermore, this method allows comparison with
237 other dune sands from the northeastern end of the Thar Desert, where we refer to earlier
238 analyses of Tripathi et al. (2004), focusing on their aeolian sand samples (n=9) from three
239 locations in the northeastern Thar Desert (Sirsa, Rohtak, and Sultanpur; Fig. 1A) and
240 fluvial samples (n=6) from the modern Sutlej River (Tripathi et al. 2004). We also
241 utilized Nd isotopic analyses from modern (n=1), Holocene (n=16), and LGM-aged (n=1)
242 fluvial sediment samples from boreholes along the lower Indus River and delta (Clift et al.
243 2002, 2008).

244 Nd isotopic compositions were analyzed for this study in 18 sediment samples,
245 including 16 fluvial samples from borehole profiles in floodplain locations at Tilwalla,
246 Yazman, Alkasur Cotton Jinnar, and Marot (in the Cholistan region of Pakistan, nearest
247 the Sutlej River and former Ghaggar-Hakra course, Fig. 1B; locations and sedimentary
248 horizons are shown in Fig. 2), one sample of modern Sutlej River sediment at Tatapani
249 (Fig. 1A), and one surface sample of aeolian sediment at Yazman. Nd isotopic content
250 was determined for the organic- and carbonate-free sediment dissolved in 8 N HF for 24
251 hr and converted to chlorides. The material was passed through cation-exchange and
252 chromatography columns to separate Nd. Samples were analyzed in dynamic mode on a

Nu® Instruments multi-collector ICP-MS at Oregon State University, and corrected for instrument bias by bracketing each sample with a J-Ndi standard (Tanaka et al. 2000) for which reproducibility was 0.000024 (2σ, n=57). Nd isotopic values are discussed in terms of ε_{Nd} (DePaolo and Wasserburg 1976), which is the $^{143}Nd/^{144}Nd$ ratio calculated relative to the Chondritic Uniform Reservoir (CHUR) standard.

RESULTS

U-Pb zircon age spectra from the three aeolian and five fluvial samples considered (Table 1; analyses from new samples in data archive table) show various proportions of zircon grains of different ages. These ages are used to infer likely derivation from Lesser Himalaya, Greater Himalaya, and Karakoram source terranes, as expected for sediment in the Indus basin (Fig. 3A). Grains younger than 300 Ma are not unique to the Karakoram range, but earlier studies have shown that this is the most important source of zircons of this age to the Indus River (Alizai et al. 2011b). Likewise, grains dating to 1700–2000 Ma are found in the Greater as well as the Lesser Himalaya, but are statistically more common in the Lesser Himalaya, so that modern rivers that drain the Lesser Himalaya tend to be much richer in 1700–2000 Ma grains that rivers that drain just the Greater Himalaya (DeCelles et al. 2000).

Although a visual comparison can be informative as to the similarity among age spectra of different samples (Fig. 3A), we quantified their similarity more rigorously by using the statistical effect size of the Kolmogorov–Smirnov (KS) test and then plotting the results using a standard statistical method known as multidimensional scaling (MDS;

see Vermeesch 2013) to produce a map (Fig. 3B) of the pattern of similarity or dissimilarity among the age spectra. The values on the axes on non-metric MDS plots simply give the rank order of similarity. This serves to group samples with similar age spectra and pull apart samples with different spectra. The accompanying Shepard plot (Fig. 3C) represents how well the MDS 'fitted distances' (distances measured with a ruler on a sheet of paper) match the true (KS) distances; the stepped line represents a transformation of the input data. If all of the reproduced distances fall onto the stepped line, then the rank ordering of distances (or similarities) has been perfectly reproduced. The stress value is a measure of the overall goodness of fit, whereby the higher the stress value the poorer the fit. Essentially, the quality of the model fit in this case is perfect. These statistical comparisons indicate that: (1) the three Thar Desert aeolian sand samples differ significantly from each other; (2) aeolian sample Chak-310, from the downwind end of the Thar Desert in Cholistan, is similar to the modern Indus River fluvial sediment at Thatta; (3) the aeolian sample UN1, from the upwind end of the desert, is statistically indistinguishable from fluvial samples from the Nara Valley, the lower Indus River–Delta at the LGM, and the lower Indus River at 7 ka; (4) the aeolian sample NM3 is statistically different from any other sample, but bears closest resemblance to the modern Indus River at Thatta; and (5) the Sutlej River sample shows an age spectrum unlike that of any other sample.

The Nd isotopic data show similarity between ε_{Nd} values of the Indus River at various time intervals and aeolian dune sand at the downwind end of the Thar Desert (Fig. 4; new analyses shown in Table 2). The ε_{Nd} range for 10 Thar Desert samples (-12 to -15.6) largely overlaps with values from the modern lower Indus River and delta (this

study and Tripathi et al. 2004); and the dune samples also overlap with the values for Holocene-aged Indus delta sediment (Fig. 4; Clift et al. 2008), although some dunes from the NE region are more negative in ε_{Nd} than most delta samples. The 16 samples analyzed from the southern Punjabi floodplain region of the Sutlej and Ghaggar-Hakra Rivers, Cholistan (Fig. 1B), show ε_{Nd} values that overlap well with those of the modern lower Indus River, the more negative end of the Holocene Indus delta, and the more negative end of the Thar Desert samples. Notably, all seven samples from the Sutlej River show ε_{Nd} values that are substantially lower than any obtained from the Indus River or Thar Desert samples (Fig. 4), even though the Sutlej River occurs in such proximity to the downwind end of the Thar Desert.

DISCUSSION

To evaluate the role of aeolian recycling in Indus basin sediment routing, provenance analysis allows us to identify the contribution of local and far-field sediment sources to Thar Desert aeolian sand. Although it might be expected that aeolian dunes at the downwind, northern end of the Thar Desert would receive most sediment from local rivers rather than from the Indus River, given the relative proximity of each, sand at the downwind end of the desert instead has greater provenance affinity with the lower Indus River and delta sediments (100s km upwind). There is remarkable similarity between the modern lower Indus River and delta region and recent aeolian dune sand even far downwind (estimated to have been deposited no earlier than 1.4 ka, based on the age of

basal aeolian dune sand at Yazman; Fig. 2), whereas the dune sand differs significantly from that of more local river sources on the southern Punjabi floodplains.

The apparent dominance of Thar Desert dune sediment from sources in the lower Indus River and delta region, based on U-Pb age spectra and ε_{Nd} patterns (Figs. 3, 4) is in agreement with earlier findings using Pb isotope analyses as a provenance tool (Alizai et al. 2011a). At Yazman and Site MGJ-5 (Fig. 1), Pb isotopes from K-feldspar grains (Alizai et al. 2011a) showed little affinity between the aeolian sands and the adjacent Sutlej River. Instead the dunes were characterized by feldspar with high $^{207}Pb/^{204}Pb$ and $^{206}Pb/^{204}Pb$ values and zircons with U-Pb crystallization ages of <100 Ma, which are typical of erosion of the Nanga Parbat metamorphic massif and arc-type sources respectively, and thus an indicator of an origin within the mainstem Indus River, not the Sutlej River. Direct reworking between the upper Indus mainstem and the desert can be ruled out on geomorphic grounds, requiring these Nanga Parbat-derived grains to have been transported fluvially to the lower reaches and then reworked to the north by wind. Thus, we infer that far-field sediment sources in the lower mainstem Indus River dominate the provenance signal in the Thar Desert samples discussed here, and attribute that dominance to wind transport. Although in some areas, bedrock outcrops within the Thar Desert also locally contribute some sediment to dunes (Wasson et al. 1983), visual field observations during this study suggest that bedrock sediment sources are important only over spatial scales of several dune lengths; bedrock sources were not observed at or immediately upwind of the Thar Desert sites sampled for this study.

Simple mixing calculations can indicate possible relative contributions to the Thar Desert samples of Indus sediment from various time intervals, or from the Sutlej

River, if any. We consider mixing relations using the available U-Pb zircon age spectra and Nd isotopic data, attempting to reconcile the proportions of modern Indus River sediment, mid-Holocene Indus delta sediment, and Indus delta sediment of LGM age that compose the Thar Desert aeolian samples at the downwind end of the desert. For the calculations that follow, we follow traditional detrital-zircon provenance techniques in presuming that the zircon populations are representative of the bulk siliciclastic content.

In order to estimate the possible contributions from different sources we consider the zircon age population split into the peaks seen in the KDE plots (Fig. 3) and attempt to reproduce the desert sand zircon populations by mixing possible end-members together. In particular we focus on the relative sizes of the age populations both in the Indus delta sediment and the Thar Desert samples. We compare zircon grains in the following groups: 0–300 Ma, 300–750 Ma, 750–1200 Ma, and 1500–2300 Ma. Other grains are removed from this calculation and the total normalized to 100% in order to simplify our mixing estimate. The <300 Ma group is especially diagnostic because it is rare in the Sutlej River sample (3% of the total zircon population), more abundant in the modern Indus River at Thatta (~23%), and very common in the Indus delta at 7 ka (49%) and at the LGM (47%). Care needs to be taken concerning the grain sizes of the material analyzed. Recent work by Yang et al. (2012) that analyzed sediments from the mainstream and tributaries of the Yangtze River revealed that younger zircons were larger or more variable in size than the older grains. This implies that there is a potential influence of hydrodynamic fractionation on zircon size and age. No specific grain-size information for our zircon samples was collected as part of this study, but, by inspection, very fine to medium sand grains dominated our data set. Yang et al. (2012) concluded

367 that the 63–125 μm size fraction yielded almost the same age population as the bulk
368 population of zircons.
369 Ideally, we would like to correct for the relative abundance of zircon grains in
370 each particular end member. This has been previously done in other zircon budgeting
371 studies that have used Zr concentration as a proxy for the relative abundance of zircon
372 crystals in different sands (Amidon et al. 2005). If we were to take that approach would
373 require assuming that the analyzed sample from each end member is representative of the
374 average composition from the Indus River at each time interval being used as an end
375 member. However, this correction may not be very accurate depending on exactly where
376 in the stream or delta the sample was taken. Hydrodynamic sorting may preferentially
377 concentrate or dilute zircon in any particular sample relative to the average flux
378 depending on where and when the sample is taken from the river channel. Although this
379 sorting is unlikely to change the ages of the zircons sampled, it can result in significant
380 variations in relative concentration over short time and length scales. Unless we know
381 that the river sand is representative of the end member at the time of sedimentation then
382 making any type of correction will introduce additional uncertainties. In view of the large
383 size of the drainage basins and therefore the unlikelihood that the source rocks are
384 significantly different in total zircon concentration because of the diversity of source
385 rocks within each sub-basin, we do not to try to correct for Zr concentration because it is
386 likely to add more uncertainty than it would resolve. In this study we estimate possible
387 contributions by mixing together end members using the relative abundances of the
388 different Indus River–Delta age populations as measured by Clift et al. (2008) and Alizai
389 et al. (2011b). It is not possible to perfectly reproduce the observed age spectra for the

390 desert sands, so we particularly focused on diagnostic populations such as those <300 Ma,
391 which are unique to the mainstem Indus River, as well as those dated at 1500–2300 Ma,
392 which are also abundant in the Sutlej River (2011b). Because the Nd isotope composition
393 is known for each of these end members, it is also possible to predict the Nd isotopic
394 composition of the Thar Desert dune sand mixed in these proportions. Unfortunately none
395 of the dune sands considered here has Nd data available, but we can compare the zircon-
396 derived budget and its predicted Nd compositions with existing Nd data from dune
397 sediment in the far northeastern part of the desert (Tripathi et al. 2004).
398 At the downwind end of the desert, sample Chak-310 contained 22% grains in the
399 age range <300 Ma, consistent with derivation from the modern or recent Indus delta that
400 contains 23.5% of such grains. Any substantial mixing with older Indus delta sediment
401 would result in much higher proportions for this age population. Conversely, receiving
402 sediment from the Sutlej River, which has virtually no zircon grains <300 Ma, would
403 substantially reduce the proportion of this age group in Thar Desert sediment. The desert
404 sand at site Chak-310 has a significant proportion of 1500–2300 Ma grains, consistent
405 with derivation from the modern Indus delta. Grains of that age are also abundant in the
406 Sutlej River, but because the latter lacks zircon grains <300 Ma, from a simple mixing
407 calculation we estimate that the Chak-310 location contains as much as 90% material
408 sourced from the modern lower Indus River, 0–10% sourced from Holocene Indus delta
409 sediment, and 0–10% from locally derived Sutlej River sediment. Such proportions
410 derived from the U-Pb zircon ages agree well with a similar mixing calculation
411 performed using ε_{Nd} values; at Yazman, Cholistan, an ε_{Nd} value of -14.5 (Table 2) is
412 consistent with having mixed modern lower Indus River sediment (average ε_{Nd} -15.3),

413 Holocene Indus delta sediment (average ε_{Nd} -13.5) and Sutlej River sediment (average
414 ε_{Nd} -17.5) in those proportions.

415 At the upwind side of the Thar Desert, samples NM3 and UN1 contain 43% and
416 40% grains in the <300 Ma age range, respectively (Table 3), suggesting that these
417 locations were influenced largely by Indus-delta sediment sources ranging in age from
418 LGM to mid-Holocene. Contribution of modern Indus sediment remains possible also,
419 although there is a dominance of mid-Holocene Indus sediment at location UN1. For
420 example, mixing calculations indicate that the zircon age spectrum for UN1 could result
421 from 55% mid-Holocene (7 ka) Indus sediment, 35% from the modern lower Indus River
422 and delta, and only 10% from the LGM delta, which predicts 40% grains <300 Ma (Fig.
423 5; Table 3). The zircon age spectrum from sample NM3 indicates proportions of 7 ka,
424 modern, and LGM Indus delta sediment of 64, 22, and 15%, respectively (Fig. 5).

425 Fluvial sands from the Nara Valley borehole that were deposited just before ~5.5
426 ka show abundant <300 Ma zircon grains (45% of the total) and some 1500–2300 Ma
427 grains (19%), and the Nara sample zircon age spectrum is statistically indistinguishable
428 from that of UN1 (which contains 45% <300 Ma and 19% 1500–2300 Ma grains),
429 suggesting interaction between mainstem Indus and Thar Desert sediment at the upwind
430 side of the desert (i.e., from Nara Valley to UN1) starting between 7.0 and 5.5 ka (Clift et
431 al. 2012). Because the samples UN1 and NM3 were collected on the surfaces of presently
432 active aeolian dunes, but do not show dominant provenance affinity with modern Indus
433 River sediment, we infer that modern dune activity in that part of the desert reworks
434 primarily older Indus and Nara fluvial sediment (cf. statistical similarity between UN1,
435 Nara, and mid-Holocene and LGM Indus samples; Fig. 3B). Because the U-Pb zircon

436 ages in the sample from active dune sand at NM3 differed from those of any other sample,
437 there may be an additional sediment source at or upwind of NM3 that we have not
438 identified.

439 The northeastern portion of the Thar Desert apparently had a somewhat different
440 provenance history than we have inferred for either the northwestern (Cholistan) region
441 or the southern region around sites NM3 and UN1. Although no zircon data are available
442 from the northeastern desert, we can compare their Nd isotopic compositions against Nd
443 isotopic compositions known for the Indus sediment sources of three time periods (gray
444 contours and shaded regions on Fig. 5). This allows us to compare sediments with only
445 zircon data to those constrained only by Nd isotopes, even if there is less certainty about
446 where in the ternary plot the Nd-based samples would place precisely.

447 The ε_{Nd} patterns at Rohtak and Sultanpur (Tripathi et al. 2004) were generally less
448 negative than the -14.5 value obtained from an aeolian dune at Yazman, in Cholistan (Fig.
449 4), although some of the dunes also show more negative values, implying either greater
450 input from the modern Indus delta (similar to Chak-310) or possibly sediment
451 contributions from local rivers such as the Sutlej or Yamuna Rivers. ε_{Nd} values of aeolian
452 dune sand in the range -12 to -14 suggest some influx of LGM-aged Indus delta material
453 (ε_{Nd} -10.8; Figs. 4, 5); the Indus delta has had ε_{Nd} values of -13 or less since ~8 ka (Clift
454 et al. 2008). The range of ε_{Nd} values in aeolian sand from the northeastern part of the
455 desert overlaps with those of the Punjabi floodplain material, as well as mainstem Indus
456 sediment of ages ranging from LGM to modern (Fig. 4). It is not practical to separate the
457 contributions from modern mainstem Indus (far-field aeolian) and Punjabi floodplain

458 (local aeolian) sources because their ε_{Nd} values are quite similar (Fig. 4), and there could
459 be substantial exchange of fluvial and aeolian sediment locally. LGM-aged Indus
460 sediment could have contributed as much as 60% (relative to modern Indus or local
461 Punjabi floodplain sources) to generate those ε_{Nd} values at the least-negative end of the
462 Thar Desert range (-12.6; Figs. 4, 5). The range of Nd isotopic values in the northeastern
463 desert suggests that any aeolian reworking of LGM-aged sediment from the Indus delta
464 into that region either was limited in volume or was subsequently diluted by isotopically
465 more negative sediments (Fig. 4).

466 Finally, we consider storage of Indus River material in the Thar Desert in the
467 context of the large Indus basin sediment-routing system. The lower Indus River and
468 delta region likely has provided sediment to Thar Desert aeolian dunes since ~8 ka (e.g.,
469 Gupta et al. 2003), when the desert expanded westward to directly adjoin the mainstem
470 Indus course on the upwind side, and possibly since the Mid-Pleistocene (Singvi et al.,
471 2010), although we have not investigated paleodune composition. The provenance signal
472 of the lower Indus River dominates at least some areas of the downwind end of the desert,
473 indicating that far-field aeolian delivery is an important sediment-transport mechanism in
474 this system, such that almost all of the aeolian sand in at least parts of the Thar Desert
475 could be derived from far-field Indus River sources (based on our mixing calculations for
476 the Chak-310 site). Thus, we consider the importance of sediment storage in the Thar
477 Desert from a volumetric standpoint relative to other sedimentary buffers in the Indus
478 basin.

479 To estimate the total sediment volume in the Thar Desert, we evaluated the
480 topographic anomaly of the desert compared to the long-wavelength sloping topography

481 of the Indus drainage basin, using SRTM (Shuttle Radar Topography Mission) data (Fig.
482 6). The land-surface elevation in the desert is somewhat higher than that which would be
483 inferred from an extrapolation of the Indus basin topography on either side of the desert,
484 and cross-sections through this elevated region can be used to infer the total sediment
485 volume in the desert. A minimum estimate can be obtained by treating the desert as a
486 simple cone of sand 200 m high with a radius of 150 km, which would indicate a volume
487 of 4700 km^3. This ignores thinner sediments in the northern region of the desert, which
488 extends >600 km along its NE-SW axis (Fig. 6). However, if we treat the SW-NE profile
489 (C–C'in Fig. 6) as being a representative cross-section along the crest of the desert
490 sediment accumulation and extending across a width of 300 km, then we would estimate
491 a total volume of ~10,600 km^3, assuming the desert sediment accumulation has a tapering
492 triangular cross-section. To be as conservative as possible, we favor the lower estimate of
493 4700 km^3. Such a sediment volume is geologically reasonable, given the distribution and
494 size of individual sand dunes in the Thar Desert, although likely an underestimate of the
495 total sediment volume. Given that Thar Desert linear dunes commonly measure 2–4 km
496 long by 0.15–0.25 km wide by 5–10 m tall in Google Earth™ aerial imagery, and that the
497 transverse and parabolic dunes commonly measure 1–3 km wide by 0.5–0.8 km long by
498 15–25 m tall, on the order of a hundred thousand dunes of such size can account for a
499 sand volume of 4700 km^3. Therefore, this seems a reasonable, if low, volume estimate for
500 the Thar Desert; our volume estimate is especially conservative given that these latter
501 calculations only account for sediment in dunes, and ignore interdune sediment and loess
502 deposits (e.g., in the Chundkho section; Fig. 2), as well as developed and irrigated regions
503 without modern dune forms. However, recycling of desert sediment into the Indus River

504 system will be most important in the western and northern regions of the Thar Desert
505 (where fluvial channels drain to the Indus), so that the entire desert sediment volume
506 would not be involved in the buffering effect we describe. Aeolian sediment blowing into
507 the eastern part of the desert could, presumably, leave the Indus watershed altogether and
508 supply sediment into the Ganges basin or the Kutch region (note eastern boundary of the
509 Indus watershed on Fig. 1A), making the Thar Desert a "leaky sink" for sediment storage.
510 Volumetrically, then, the Thar Desert stores three orders of magnitude less
511 sediment than does the Indus submarine fan (4,700 km^3 vs. 5,000,000 km^3; Naini and
512 Kolla 1982). Although the desert is a minor sediment sink compared to the ultimate
513 marine sink, the desert stores a greater sediment volume than all other known sediment-
514 storage locales in the Indus Basin combined (Fig. 7). The desert represents a much larger
515 sediment sink, for example, than does sediment storage in Himalayan valley fills of the
516 Indus basin headwaters (~250–270 km^3; Blöthe and Korup 2013; Clift and Giosan, 2014).
517 Lag times also could be substantially longer for sediment in the Thar Desert, perhaps as
518 long as 10^6 yrs (cf. Vermeesch et al. 2010), whereas Himalayan valley fill has sediment
519 residence times of 10^3–10^5 yr (Blöthe and Korup 2013)—although the inference of
520 modern Indus-composition sand in Cholistan suggests residence times in the Thar Desert
521 could be as short as 10^3 yr. The sediment volume in the Thar Desert is also at least twice
522 as large as the sediment volume deposited since the LGM in the largest alluvial segment
523 of the mainstem Indus River (725–2500 km^3 in the Sindh alluvial plain; Clift and Giosan
524 2014). Therefore, we conclude that aeolian transport of river material into temporary
525 storage in the desert introduces a volumetrically and probably temporally important
526 buffer to the sediment-transfer zone. It is likely that fluvial–aeolian interactions affect

sediment routing in other dryland systems as well, but that this process has not been widely recognized in the literature. Although the Thar Desert is inferred to be a substantial buffer of sediment being transported toward the Arabian Sea, this process is likely variable through geologic time. Northeastward aeolian sediment-transport potential is presumably greatest during times when the summer monsoon winds are strong, such as during the mid-Holocene (11–6 ka; Sirocko et al. 1996). In contrast, the last glacial episode was characterized by weaker summer monsoon winds and, we surmise, probably less aeolian sediment recycling.

CONCLUSIONS

Isotopic similarities between Indus River fluvial sediment and Thar Desert aeolian sediment indicate that the majority of sediment in the sampled desert regions is derived from wind-reworked fluvial deposits of the lower Indus River and delta. Sediment storage in the desert thus can be considered to buffer, or delay, sediment transfer from the Himalayas to the Indus submarine fan, potentially affecting transmission of environmental signals to the marine stratigraphic record. Although sediment storage in the Thar Desert is volumetrically small relative to the marine sedimentary sink (the Indus fan), it is important to recognize fluvial-aeolian cycling as a process that can interrupt the transfer of sediment-flux signals to the marine record, for at least a small proportion of the sediment in the Indus transfer system. The sediment volume stored in the desert is inferred to be nearly 20 times greater than that of alluvial and mass-wasting deposits that store sediment in the Himalayan headwater regions of the Indus basin, is at least twice as great as the largest alluvial-plain segment of the mainstem Indus River, and is greater

than the combined volume of all other known sediment buffer zones in the Indus sediment-routing system. Residence times of Indus sediment in the Thar Desert are likely comparable to or longer than lag times in alluvial buffering systems. The importance of this recycling between the fluvial and aeolian system must vary through time depending on the size of the desert, the transport capacity of summer monsoon winds, and sediment supply from the Himalaya, all of which are linked to monsoon intensity and in turn to glacial-interglacial cycles.

ACKNOWLEDGMENTS

PDC thanks the Charles T. McCord chair fund at LSU for assistance in undertaking this work. The authors thank L. Giosan for valuable discussions. J.K. Tripathi kindly provided quantitative Nd isotopic data that were not explicitly presented by Tripathi et al. (2004). E. Hajek, R. Wasson, and J. Warrick provided insightful and constructive review comments that improved the manuscript. We thank J. Gillies and J. MacEachern for their editorial work.

565

566 **REFERENCES**

567

568 ALIZAI, A., CLIFT, P.D., GIOSAN, L., VANLANINGHAM, S., HINTON, R., TABREZ, A.R.,
569 DANISH, M., AND EIMF, 2011a, Pb Isotopic Variability in the Modern and Holocene
570 Indus River System measured by Ion Microprobe in detrital K-feldspar grains:
571 Geochimica et Cosmochimica Acta, v. 75, p. 4771–4795.

572 ALIZAI, A., CARTER, A., CLIFT, P.D., VANLANINGHAM, S., WILLIAMS, J.C., AND KUMAR,
573 R., 2011b, Sediment provenance, reworking and transport processes in the Indus
574 River by U–Pb dating of detrital zircon grains: Global and Planetary Change, v. 76, p.
575 33–55.

576 AMIDON, W. H., BURBANK, D. W., AND GEHRELS, G. E., 2005, Construction of detrital
577 mineral populations: insights from mixing of U-Pb zircon ages in Himalayan rivers:
578 Basin Research, v. 17, no. 4, p. 463-485.

579 AMIT, R., ENZEL, Y., CROUVI, O., SIMHAI, O., MATMON, A., PORAT, N., MCDONALD, E.,
580 AND GILLESPIE, A.R., 2011, The role of the Nile in initiating a massive dust influx to
581 the Negev late in the middle Pleistocene: Geological Society of America, Bulletin, v.
582 123, p. 873–889.

583 ARMITAGE, J.J., JONES, T.D., DULLER, R.A., WHITTAKER, A.C., AND ALLEN, P.A., 2013,
584 Temporal buffering of climate-driven sediment flux cycles by transient catchment
585 response: Earth and Planetary Science Letters, v. 369–370, p. 200–210.

586 BELNAP, J., MUNSON, S.M., AND FIELD, J.P., 2011, Aeolian and fluvial processes in
587 dryland regions: the need for integrated studies: Ecohydrology, v. 4, p. 615–622.

588 BLACK, L.P., KAMO, S.L., ALLEN, C.M., ALEINIKOFF, J.N., DAVIS, D.W., KORSCH, R.J.,
589 AND FOUDOULIS, C., 2003, TEMORA 1: a new zircon standard for Phanerozoic U–Pb
590 geochronology: Chemical Geology, v. 200, no. 1–2, p. 155–170.
591 BLÖTHE, J.H., AND KORUP, O., 2013, Millennial lag times in the Himalayan sediment
592 routing system: Earth and Planetary Science Letters, v. 382, p. 38–46.
593 BULLARD, J.E., AND LIVINGSTONE, I., 2002, Interactions between aeolian and fluvial
594 systems in dryland environments: Area, v. 34.1, p. 8–16.
595 BULLARD, J.E., AND MCTAINSH, G.H., 2003, Aeolian-fluvial interactions in dryland
596 environments: examples, concepts, and Australia case study: Progress in Physical
597 Geography, v. 27, p. 471–501.
598 CARTER, A., AND BRISTOW, C.S., 2001, Detrital zircon geochronology: enhancing the
599 quality of sedimentary source information through improved methodology and
600 combined U–Pb and fission-track techniques. Basin Research, v. 12, p. 47–57.
601 CASTELLTORT, S., AND VAN DEN DRIESSCHE, J., 2003, How plausible are high-frequency
602 sediment supply-driven cycles in the stratigraphic record?: Sedimentary Geology, v.
603 157, p. 3–13.
604 CLIFT, P.D., AND GIOSAN, L., 2014, Sediment fluxes and buffering in the post-glacial
605 Indus Basin: Basin Research, DOI: 10.1111/bre.12038
606 CLIFT, P.D., CARTER, A., GIOSAN, L., DURCAN, J., TABREZ, A. R., ALIZAI, A.,
607 VANLANINGHAM, S., DULLER, G. A. T., MACKLIN, M. G., FULLER, D. Q., AND
608 DANISH, M., 2012, U-Pb zircon dating evidence for a Pleistocene Sarasvati River and
609 Capture of the Yamuna River: Geology, v. 40, p. 212-215.

610 CLIFT, P.D., GIOSAN, L., BLUSZTAJN, J., CAMPBELL, I.H., ALLEN, C., PRINGLE, M.,
611 TABREZ, A.R., DANISH, M., RABBANI, M.M., ALIZAI, A., CARTER, A., AND LÜCKGE,
612 A., 2008, Holocene erosion of the Lesser Himalaya triggered by intensified summer
613 monsoon: Geology, v. 36, p. 79–82.
614 CLIFT, P.D., CAMPBELL, I.H., PRINGLE, M.S., CARTER, A., ZHANG, X., HODGES, K.V.,
615 KHAN, A.A., AND ALLEN, C.M., 2004, Thermochronology of the modern Indus River
616 bedload; new insight into the control on the marine stratigraphic record: Tectonics, v.
617 23, TC5013.
618 CLIFT, P.D., LEE, J.I., HILDEBRAND, P., SHIMIZU, N., LAYNE, G.D., BLUSZTAJN, J., BLUM,
619 J.D., GARZANTI, E., KHAN, A.A., 2002, Nd and Pb isotope variability in the Indus
620 River system; implications for sediment provenance and crustal heterogeneity in the
621 western Himalaya. Earth and Planetary Science Letters, 200(1-2): 91-106.
622 DECELLES, P.G., GEHRELS, G.E., QUADE, J., LAREAU, B., AND SPURLIN, M., 2000,
623 Tectonic implications of U-Pb zircon ages of the Himalayan orogenic belt in Nepal:
624 Science, v. 288, p. 497–499.
625 DEPAOLO, D.J., AND WASSERBURG, G.J., 1976, Nd isotopic variations and petrogenetic
626 models: Geophysical Research Letters, v. 3, p. 249–252.
627 DRAUT, A.E., 2012, Effects of river regulation on aeolian landscapes, Colorado River,
628 southwestern USA: Journal of Geophysical Research, v. 117, F2,
629 doi:10.1029/2011JF002329.
630 DUNNE, T., MERTES, L.A.K., MEADE, R.H., RICHEY, J.E., AND FORSBERG, B.R., 1998,
631 Exchanges of sediment between the flood plain and channel of the Amazon River in
632 Brazil: Geological Society of America Bulletin, v. 110, p. 450–467.

633 DURCAN, J.A., ROBERTS, H.M., DULLER, G.A.T., AND ALIZAI, A.H., 2010, Testing the
634 use of range-finder OSL dating to inform field sampling and laboratory processing
635 strategies: Quaternary Geochronology, v. 5, p. 86–90.
636 FORZONI, A., STORMS, J.E.A., WHITTAKER, A.C., AND DE JAGER, G., 2014, Delayed
637 delivery from the sediment factory: modeling the impact of catchment response time
638 to tectonics on sediment flux and fluvio-deltaic stratigraphy: Earth Surface Processes
639 and Landforms, v. 39, p. 689–704.
640 FRASER, J.E., SEARLE, M.P., PARRISH, R.R., AND NOBLE, S.R., 2001, Chronology of
641 deformation, metamorphism, and magmatism in the southern Karakoram Mountains:
642 Geological Society of America Bulletin, v. 113, p. 1443–1455.
643 GEHRELS, G.E., DECELLES, P.G., OJHA, T.P., AND UPRETI, B.N., 2006, Geologic and U-
644 Th-Pb geochronologic evidence for early Paleozoic tectonism in the Kathmandu
645 thrust sheet, central Nepal Himalaya: Geological Society of America Bulletin, v. 118,
646 p. 185–198.
647 GIBLING, M.R., SINHA, R., ROY, N.G., TANDON, S.K., AND JAIN, M., 2008. Quaternary
648 fluvial and eolian deposits on the Belan river, India: paleoclimatic setting of
649 Paleolithic to Neolithic archeological sites over the past 85,000 years: Quaternary
650 Science Reviews, v. 27, p. 391–410.
651 GIOSAN, L., CLIFT, P. D., BLUSZTAJN, J., TABREZ, A., CONSTANTINESCU, S., AND FILIP, F.,
652 2006, On the control of climate- and human-modulated fluvial sediment delivery on
653 river delta development: The Indus: Eos, Transactions, American Geophysical Union,
654 v. 87, no. 52, p. OS14A-04.

655 GIOSAN, L., CLIFT, P.D., MACKLIN, M.G., FULLER, D.Q., CONSTANTINESCU, S., DURCAN,
656 J. A., STEVENS, T., DULLER, G. A. T., TABREZ, A., ADHIKARI, R., GANGAL, K.,
657 ALIZAI, A., FILIP, F., VANLANINGHAM, S., AND SYVITSKI, J.P.M., 2012, Fluvial
658 Landscapes of the Harappan Civilization: Proceedings of the National Academy of
659 Sciences, v. 109, no. 26, p. 1688-1694.
660 GLENNIE, K.W., SINGHVI, A.K., LANCASTER, N., AND TELLER, J.T., 2002, Quaternary
661 climatic changes over Southern Arabia and the Thar Desert, India, *in* Clift, P.D.,
662 Kroon, D., Gaedicke, C., and Craig, J., eds., The tectonic and climatic evolution of
663 the Arabian Sea region, Volume 195: London, Geological Society, p. 301-316.
664 GOODBRED, S.L., 2003, Response of the Ganges dispersal system to climate change: a
665 source-to-sink view since the last interstade: Sedimentary Geology, v. 162, p. 83–103.
666 GUPTA, A.K., ANDERSON, D.M., AND OVERPECK, J.T., 2003, Abrupt changes in the Asian
667 southwest monsoon during the Holocene and their links to the North Atlantic Ocean:
668 Nature, v. 421, p. 354–356.
669 HAN, G., ZHANG, G., AND DONG, Y., 2007, A model for the active origin and
670 development of source-bordering dunefields on a semiarid fluvial plan: a case study
671 from the Xiliaohe Plain, Northeast China: Geomorphology, v. 86, p. 512–524.
672 HODGES, K.V., PARRISH, R.R., AND SEARLE, M.P., 1996, Tectonic evolution of the
673 central Annapurna Range, Nepalese Himalayas: Tectonics, v. 15, p. 1264–1291.
674 KAMESWARA RAO, K., WASSON, R.J., AND KUTTY, M.K., 1989, Foraminifera from Late
675 Quaternary dune sands of the Thar Desert, India: Palaios, v. 4, p. 168–180.
676 KAR, A., 1993, Aeolian processes and bedforms in the Thar desert: Journal of Arid
677 Environments, v. 25, p. 83–96.

LE FORT, P., DEBON, F., AND SONET, J., 1983, Petrography, geochemistry, and geochronology of some samples from the Karakoram Batholith (N. Pakistan), *in* Shams, F.A., ed., Granites of the Himalayas, Karakoram and Hindu Kush: Lahore, Pakistan, Punjab University, p. 377–387.

MUHS, D.R., REYNOLDS, R.L., BEEN, J., AND SKIPP, G., 2003, Eolian sand transport pathways in the southwestern United States: importance of the Colorado River and local sources: Quaternary International, v. 104, p. 3–18.

NAINI, B.R., AND KOLLA, V., 1982, Acoustic character and thickness of sediments of the Indus Fan and the continental margin of western India: Marine Geology, v. 47, p. 181–185.

PARRISH, R.R., AND TIRRUL, R., 1989, U-Pb age of the Baltoro Granite, Northwest Himalaya, and implications for monazite U-Pb systematics: Geology, v. 17, p. 1076–1079.

PARRISH, R.R., AND HODGES, K.V., 1996, Isotopic constraints on the age and provenance of the Lesser and Greater Himalyan sequences, Nepalese Himalaya: Geological Society of America Bulletin, v. 108, p. 904–911.

PEARCE, N.J.G., PERKINS, W.T., WESTGATE, J.A., GORTON, M.P., JACKSON, S.E., NEAL, C.R., AND CHENERY, S.P., 1997, A compilation of new and published major and trace element data for NIST SRM 610 and NIST SRM 612 glass reference materials. Geostandards Newsletter, v. 21, p. 115–144.

PETTER, A.L., STEEL, R.J., MOHRIG, D., KIM, W., AND CARVAJAL, C., 2013, Estimation of the paleoflux of terrestrial-derived solids across ancient basin margins using the stratigraphic record: Geological Society of America Bulletin, v. 125, p. 578–593.

701 PIZZUTO, J.E., 2014, Long-term storage and transport length scale of fine sediment:
702 analysis of a mercury release into a river: Geophysical Research Letters, in press.
703 PRINS, M.A., ZHENG, H., BEETS, K., TROELSTRA, S., BACON, P., KAMERLING, I., WESTER,
704 W., KONERT, M., HUANG, X., KE, W., AND VANDENBERGHE, J., 2009, Dust supply
705 from river floodplains: the case of the lower Huang He (Yellow River) recorded in a
706 loess-palaeosol sequence from the Mangshan Plateau: Journal of Quaternary
707 Science, v. 24, p. 75–84.
708 RAMSEY, M.S., CHRISTENSEN, P.R., LANCASTER, N., AND HOWARD, D.A., 1999,
709 Identification of sand sources and transport pathways at the Kelso Dunes, California,
710 using thermal infrared remote sensing: Geological Society of America Bulletin, v.
711 111, p. 646–662.
712 REIMER, P.J., BAILLIE, M.G.L., BARD, E., BAYLISS, A., BECK, J.W., BERTRAND, C.J.H.,
713 BLACKWELL, P.G., BUCK, C.E., BURR, G.S., CUTLER, K.B., DAMON, P.E.,
714 EDWARDS, R.L., FAIRBANKS, R.G., FRIEDRICH, M., GUILDERSON, T.P., HOGG, A.G.,
715 HUGHEN, K.A., KROMER, B., MCCORMAC, G., MANNING, S., RAMSEY, C.B.,
716 REIMER, R.W., REMMELE, S., SOUTHON, J.R., STUIVER, M., TALAMO, S., TAYLOR,
717 F.W., VAN DER PLICHT, J., AND WEYHENMEYER, C.E., 2004, IntCal04 terrestrial
718 radiocarbon age calibration, 0–26 cal kyr BP: Radiocarbon, v. 46, p. 1029–1058.
719 ROSKIN, J., KATRA, I., AGHA, N., GORING-MORRIS, A.N., PORAT, N., AND BARZILAI, O.,
720 2014, Rapid anthropogenic response to short-term aeolian-fluvial
721 palaeoenvironmental changes during the Late Pleistocene–Holocene transition in
722 the northern Negev Desert, Israel: Quaternary Science Reviews, v. 99, p. 176–192.

723 SAINI, H.S., TANDON, S.K., MUJTABA, S.A.I., PANT, N.C., AND KHORANA, R.K., 2009,
724 Reconstruction of buried channel-floodplain systems of the northwestern Haryana
725 Plains and their relation to the 'Vedic' Saraswati. Current Science, v. 97, p. 1634–
726 1643.
727 SCHÄRER, U., COPELAND, P., HARRISON, T.M., AND SEARLE, M.P., 1990, Age, cooling
728 history, and origin of post-collisional leucogranites in the Karakoram Batholith; a
729 multi-system isotope study: Journal of Geology, v. 98, 233–251.
730 SEARLE, M.P., PARRISH, R.R., TIRRUL, R., AND REX, D.C., 1990, Age of crystallization of
731 the K2 gneiss in the Baltoro Karakoram: Journal of the Geological Society, v. 147,
732 p. 603–606.
733 SIMPSON, G., AND CASTELLTORT, S., 2012, Model shows that rivers transmit high-
734 frequency climate cycles to the sedimentary record: Geology, v. 40, p. 1131–1134.
735 SINGHVI, A.K., WILLIAMS, M.A.J., RAJAGURU, S.N., MISRA, V.N., CHAWLA, S., STOKES,
736 S., CHAUHAN, N., FRANCIS, T., GANJOO, R.K., AND HUMPHREYS, G. S., 2010, A 200
737 ka record of climatic change and dune activity in the Thar Desert, India: Quaternary
738 Science Reviews, v. 29, no. 23–24, p. 3095–3105.
739 SINGHVI, A.K., AND KAR, A., 2004, The aeolian sedimentation record of the Thar desert:
740 Proceedings of the Indian Academy of Sciences, v. 113, no. 3, p. 371–401.
741 SIROCKO, F., GARBE-SCHÖNBERG, D., MCINTYRE, A., AND MOLFINO, B., 1996,
742 Teleconnections between the subtropical monsoons and high-latitude climates during
743 the last deglaciation: Science, v. 272, p. 526–529.

744 SLÁMA, J., KOSLER, J., CONDON, D.J., ET AL., 2008, Plezovice zircon: a new natural
745 reference material for U–Pb and Hf isotopic microanalysis: Chemical Geology, v. 249,
746 p. 1–35.
747 STUIVER, M., REIMER, P.J., BARD, E., BECK, J.W., BURR, K.A., HUGHEN, K.A., KROMER,
748 B., MCCORMAC, J., VAN DER PLICHT, J., AND SPURK, M., 1998, INTCAL98
749 radiocarbon age calibration: Radiocarbon, v. 40, p. 1041–1083.
750 TANAKA, T., TOGASHI, S., KAMIOKA, H., AMAKAWA, H., KAGAMI, H., HAMAMOTO, T.,
751 YUHARA, M., ORIHASHI, Y., YONEDA, S., SHIMIZU, H., KUNIMARU, T., TAKAHASHI,
752 K., YANAGI, T., NAKANO, T., FUJIMAKI, H., SHINJO, R., ASAHARA, Y., TANIMIZU, M.,
753 AND DRAGUSANU, C., 2000, JNdi-1: a neodymium isotopic reference in consistency
754 with La Jolla neodymium: Chemical Geology, v. 168, p. 279–281.
755 TRIMBLE, S.W., 1983, A sediment budget for Coon Creek basin in the Driftless Area,
756 Wisconsin, 1853–1977: American Journal of Science, v. 283, p. 454–474.
757 TRIPATHI, J.K., BOCK, B., RAJAMANI, V., AND EISENHAUER, A., 2004. Is River Ghaggur,
758 Saraswati? Geochemical constraints: Current Science, v. 87, p. 1141-1145.
759 VALDIYA, K. S., 2002. Saraswati: The River that Disappeared: 1st University Press
760 (India) Limited, Hyderabad, India., 116 pp.
761 VERMEESCH, P., FENTON, C.R., KOBER, F., WIGGS, G.F.S., BRISTOW, C.S., AND XU, S.,
762 2010, Sand residence times of one million years in the Namib Sand Sea from
763 cosmogenic nuclides: Nature Geoscience, v. 3, p. 862–865, doi:10.1038/NGEO985.
764 VERMEESCH, P., 2004, How many grains are needed for a provenance study?: Earth and
765 Planetary Science Letters, v. 224, p. 351–441.

766 VERMEESCH, P., 2012, On the visualisation of detrital age distributions: Chemical
767 Geology, v. 312–313, p. 190–194.
768 VERMEESCH, P., 2013, Multi-sample comparison of detrital age distributions: Chemical
769 Geology, v. 341, p. 140–146.
770 WASSON, R.J., RAJAGURU, S.N., MISRA, V.N., AGRAWAL, D.P., DHIR, R.P., SINGHVI,
771 A.K., AND KAMESWARA RAO, K., 1983, Geomorphology, late Quaternary stratigraphy,
772 and paleoclimatology of the Thar dune field: Zeitschrift für Geomorphologie. Annals
773 of Geomorphology. Supplement Volumes, v. 45, p. 117–151.
774 WIEDENBECK, M., HANCHAR, J.M., PECK, W.H., SYLVESTER, P., VALLEY, J.,
775 WHITEHOUSE, M., KRONZ, A., MORISHITA, Y., NASDALA, L., FIEBIG, J., FRANCHI, I.,
776 GIRARD, J.-P., GREENWOOD, R.C., HINTON, R., KITA, N., MASON, P.R.D., NORMAN,
777 M., OGASAWARA, M., PICCOLI, P.M., RHEDE, D., SATOH, H., SCHULZ-DOBRICK, B.,
778 SKÅR, O., SPICUZZA, MJ., TERADA, K., TINDLE, A., TOGASHI, S., VENNEMANN, T.,
779 XIE, Q. AND ZHEN, Y.-F., 2004, Further characterization of the 91500 zircon crystal:
780 Geostandards and Geoanalytical Research, v. 28, p. 9-39, doi: 10.1111/j.1751-
781 908X.2004.tb01041.
782 WOLINSKY, M.A., SWENSON, J.B., LITCHFIELD, N., AND MCNINCH, J.E., 2010, Coastal
783 progradation and sediment partitioning in the Holocene Waipaoa sedimentary system,
784 New Zealand: Marine Geology, v. 270, p. 94–107.
785 YANG, S., ZHANG, F. AND WANG, Z., 2012. Grain size distribution and age population of
786 detrital zircons from the Changjiang (Yangtze) River system, China: Chemical
787 Geology, v. 296-297, p. 26-38.
788

FIGURE CAPTIONS

Figure 1. (A) Location map shows regional context of the Indus River catchment, major tributaries, the Thar Desert, and locations discussed in the text. Boxes show areas covered in Fig. 1B and 1C. The Punjabi floodplains comprise the Sutlej and Ghaggar-Hakra (G-H) Rivers and other adjacent channels. Image courtesy of Google Earth. The site at Tatapani included both a pre-existing zircon U–Pb analysis (Alizai et al. 2011a) and newly analyzed Nd isotopic data for the Sutlej River (this study). (B) False-color image of a portion of the northwestern downwind end of the Thar Desert and Sutlej River course, in Cholistan. (C) False-color image of the Nara Valley, western Thar Desert. Aeolian dunes are in pink; prevailing wind direction is toward north-northeast. Images in (B) and (C) courtesy of NASA Worldwind. Green circles, sample locations of Nd isotope data from Tripathi et al. (2004); yellow circles, sample locations of new Nd isotope data (this study); blue squares, sample locations for U-Pb zircon data of Clift et al. (2008) and Alizai et al. (2011b); pink squares, sample locations for new U-Pb zircon data (this study); white circles, boreholes and stratigraphic sections shown in Fig. 2 that are not already represented by one of the aforementioned symbols.

Figure 2. Sedimentary profiles from the Thar Desert, Nara Valley, Sutlej River valley, and lower Indus River and delta. Section from Chamu is from Singhvi and Kar (2004). Section from Thatta is from Clift et al. (2008). Sections from Marot, Yazman, Fakirabad, Nara drill site are from Alizai et al. (2011a). Section from Tilwalla is from Clift et al. (2012). Sections from Alkasur Cotton Jinner, MGJ-5, and Nara Kenab are from Giosan et

al. (2012). Section from Chak 310, this study (zircon sample analyzed by Alizai et al., 2011b). Section from Chundkho, this study. See Fig. 1 for locations. Ages indicated by sedimentary horizons were determined by optically stimulated luminescence (OSL) where indicated; other ages were determined by accelerator mass spectrometry (AMS) radiocarbon dating of organic material and mollusk shells at the National Ocean Sciences Accelerator Mass Spectrometry Facility (NOSAMS) at the Woods Hole Oceanographic Institution, Massachusetts, USA (http://nosams.whoi.edu); dates were converted to calendar ages using the IntCal04 calibration dataset (Reimer et al. 2004) for plant matter and Calib 5.0.1 software for mollusk shells (Stuiver et al. 1998).

Figure 3. Results of detrital-zircon U-Pb age-spectra comparisons. (A) Kernel Density Estimation (KDE) plots for U-Pb ages in detrital zircon grains from the Thar Desert, the modern Indus and Sutlej Rivers, the Nara River before 5.5 ka, as well as the Indus River mouth at 7 ka and at ~20 ka. Data sources as shown in Table 1. Characteristic age ranges are shown for the Karakoram source terrane (Le Fort et al. 1983; Parrish and Tirrul 1989; Schärer et al. 1990; Searle et al. 1990; Fraser et al. 2001), Greater Himalayas (Noble and Searle 1995; Hodges et al. 1996; Parrish and Hodges 2006; DeCelles et al. 2000; Gehrels et al. 2006), and Lesser Himalayas (Parrish and Hodges 1996; DeCelles et al. 2000). (B) Multidimensional scaling (MDS) mapping (cf. Vermeesch, 2013) groups samples with similar age spectra, and separates samples with different spectra. Values on the axes are units of space. (C) 'Shepard plot' provides a graphical assessment of MDS model fit, which is essentially perfect in this case; see text for further description.

835 Figure 4. Kernel Density Estimation (KDE) plot of ε_{Nd} values for the Thar Desert and
836 other possible sediment sources. Thar Desert aeolian sand data and Sutlej River sand data
837 from Tripathi et al. (2004). Holocene and LGM lower Indus delta data are from sand
838 samples in boreholes studied by Clift et al. (2008), largely at Keti Bundar (location on Fig.
839 1A). Modern lower Indus River sand value from Thatta (-15.5) and just below the
840 confluence of the Indus and Sutlej Rivers (-15.1) are from Clift et al. (2002). Punjabi
841 floodplains data, this study.
842
843 Figure 5. Ternary diagram showing possible mixing relationships among different
844 compositions of the mainstem Indus River–delta region at three time periods: the last
845 glacial maximum (LGM), 7 ka, and modern time. Black dots show the estimated
846 contributions of Indus sediment of these three ages in three Thar Desert dune samples
847 based on zircon age spectra, whereas gray contours show the ε_{Nd} values that would be
848 associated with these mixtures. Gray shaded regions indicate estimates for sediments for
849 which only Nd isotope data (but not zircon data) are available. See text and Table 3 for
850 data sources.
851
852 Figure 6. Topographic profiles across the Thar Desert, from SRTM (Shuttle Radar
853 Topography Mission) data (www.geomapapp.org), showing the mounding of desert
854 topography over a regional slope for this part of the Indus basin, inferred as shown by the
855 dashed lines. Topography above the dashed line is presumed to represent desert sediment.
856

857 Figure 7. Relative proportions of sediment stored in the Thar Desert (from a conservative
858 volume estimate) compared to other temporary sediment stores in the Indus basin, all of
859 which have contributed reworked sediment to the Indus delta since the last glacial
860 maximum (LGM; Clift and Giosan, 2014). Terrace deposits in mountainous regions
861 include both fluvial deposits and lesser volumes of mass-wasted material (Blöthe and
862 Korup, 2013).
863
864 Table 1. Samples from which U-Pb zircon data are available for tracing provenance
865 history among the Thar Desert, Indus River, and adjacent tributary basins (Sutlej River
866 and Nara Valley).
867
868 Table 2. Results of Nd isotopic analyses (presented as relative frequency of ε_{Nd} values),
869 showing new and previously published data. New data include one measurement from the
870 modern Sutlej River at Tatapani (sample S3), and 17 from the southern Punjabi
871 floodplain region of the Sutlej and Ghaggar-Hakra river courses. Of the latter 17, Sample
872 S4-081109-18 is aeolian sediment, all others are fluvial.
873
874 Table 3. Percentages of different age groups in U-Pb zircon age spectra for Indus River
875 end-member sediment sources from three time periods (LGM, 7 ka, and modern)
876 considered in mixing calculations, together with the relative abundance in three Thar
877 Desert dune sand samples for which zircon data are available (NM3, UN1, and Chak-
878 310). Also shown are Nd isotope compositions (ε_{Nd} values) for the end members.
879

Data Archive Table. U-Pb zircon data for UN1, NM3, and Nara-1 drill site (see Table 1 for sample descriptions).

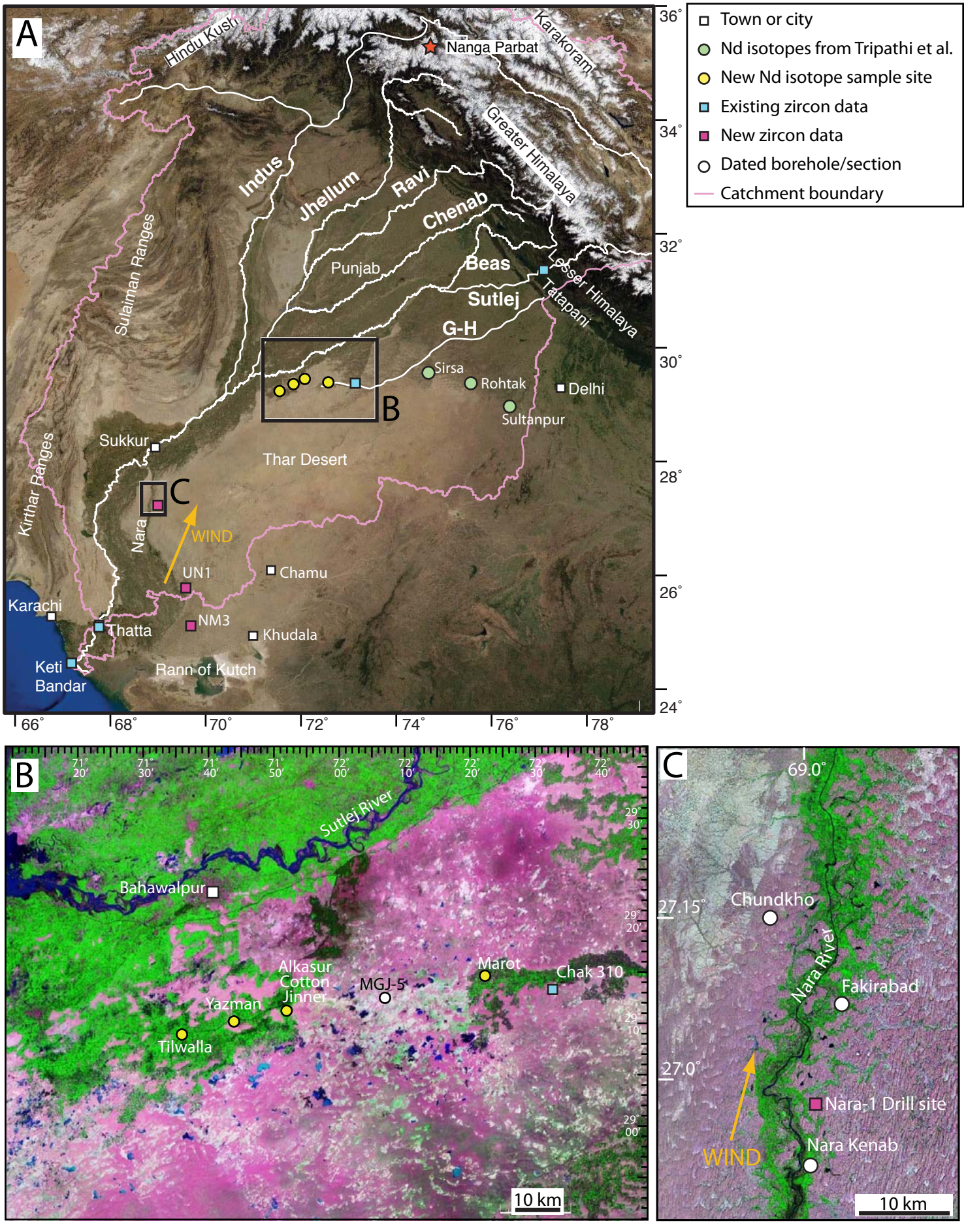

Figure 1
East et al.

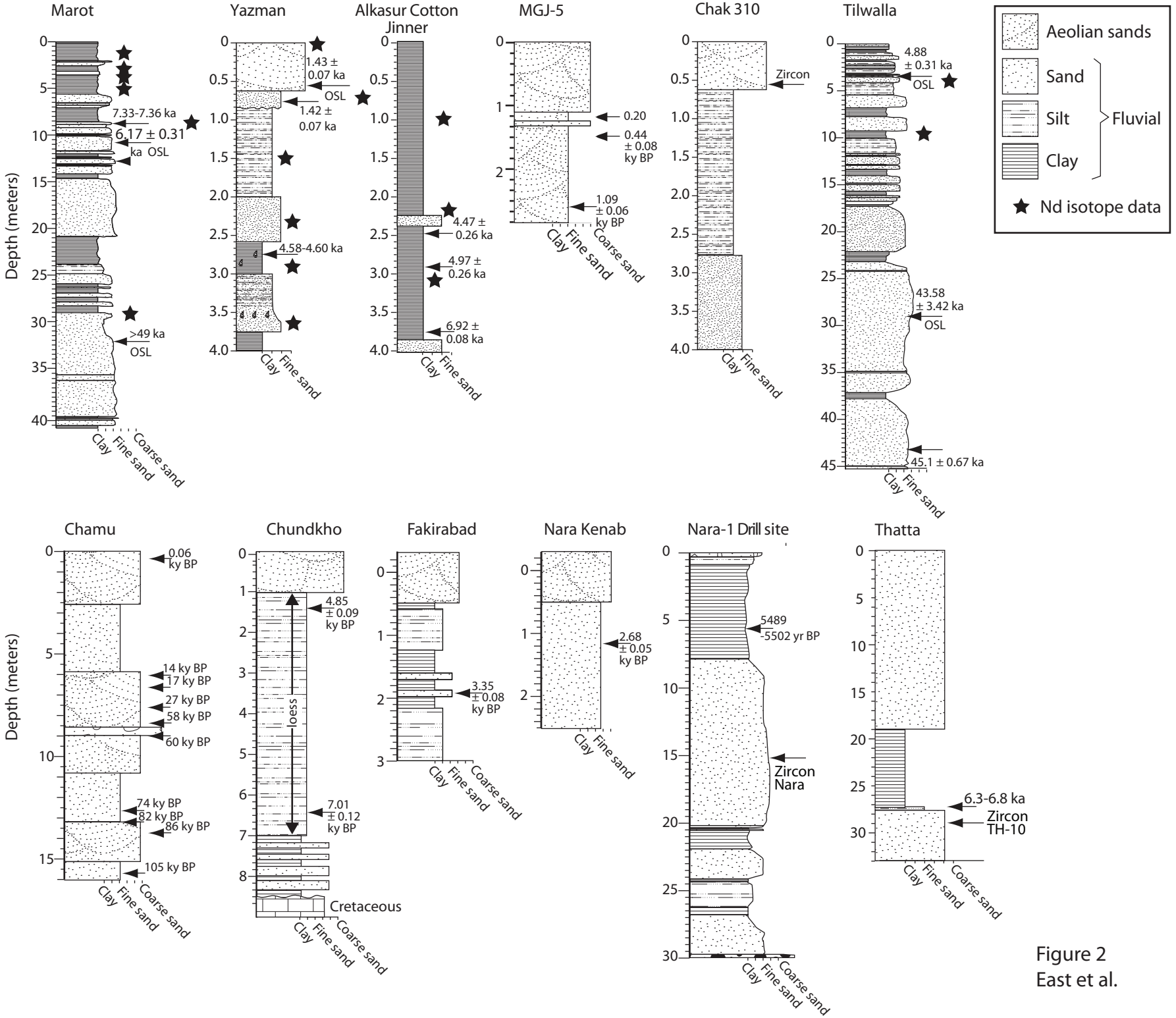

Figure 2
East et al.

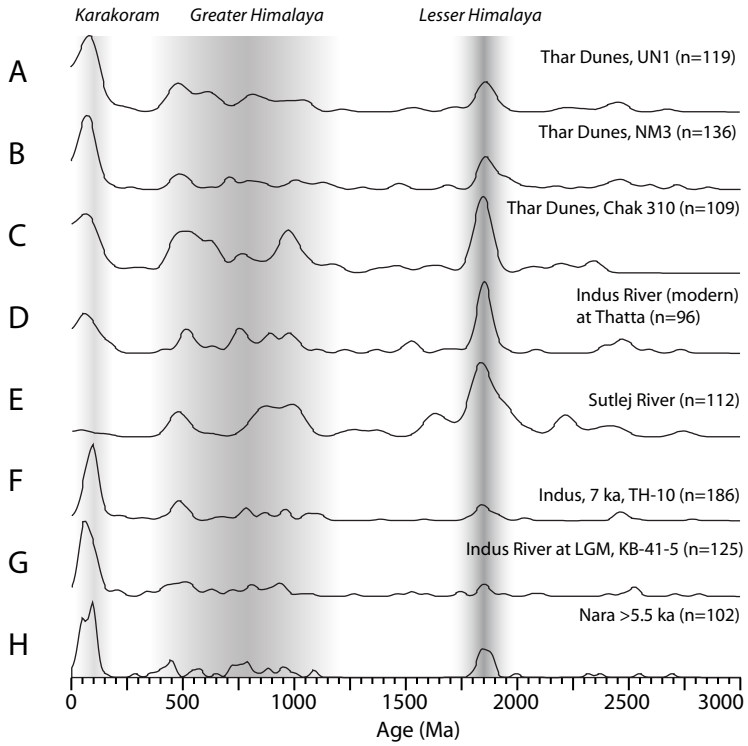

Figure 3
East et al.

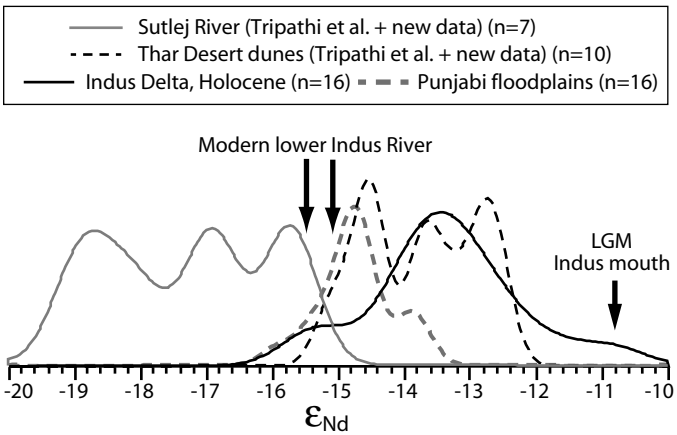

Figure 4
East et al.

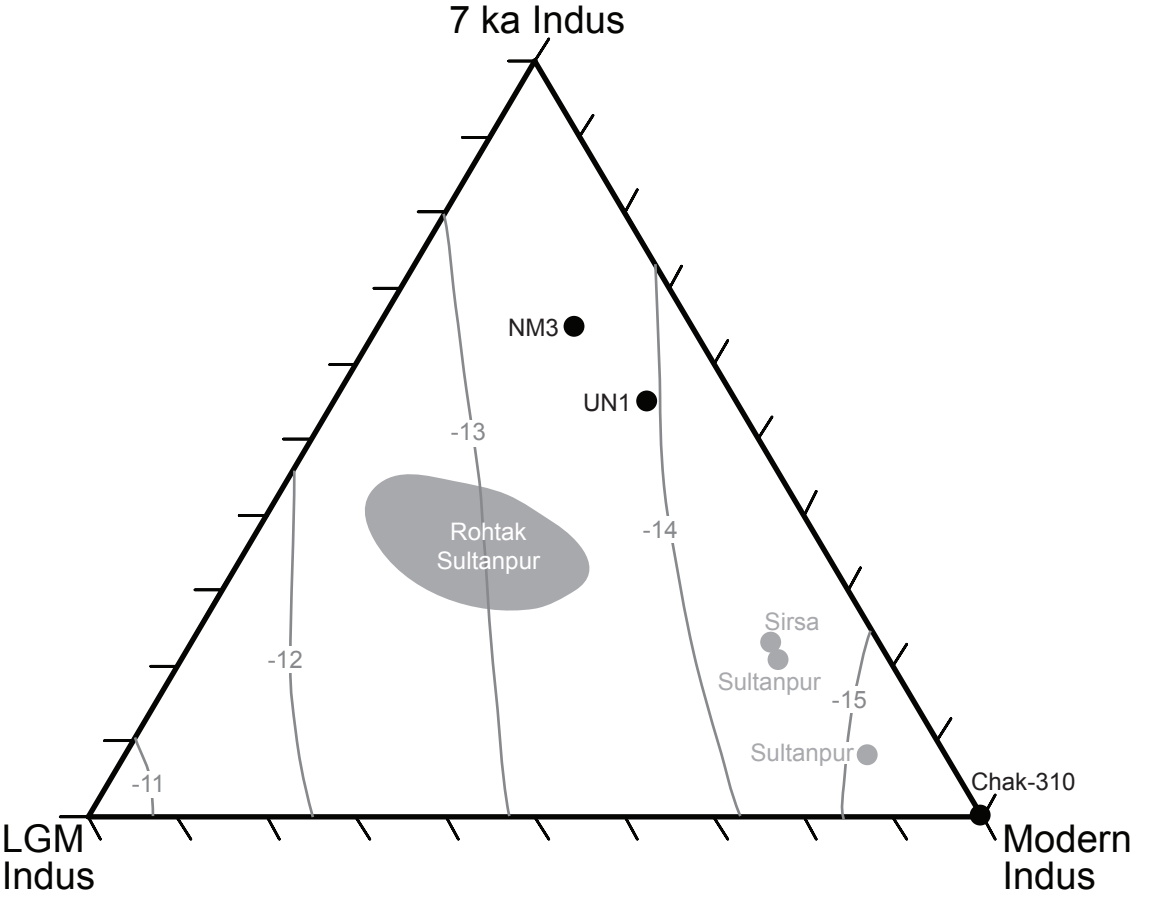

Figure 5
East et al.

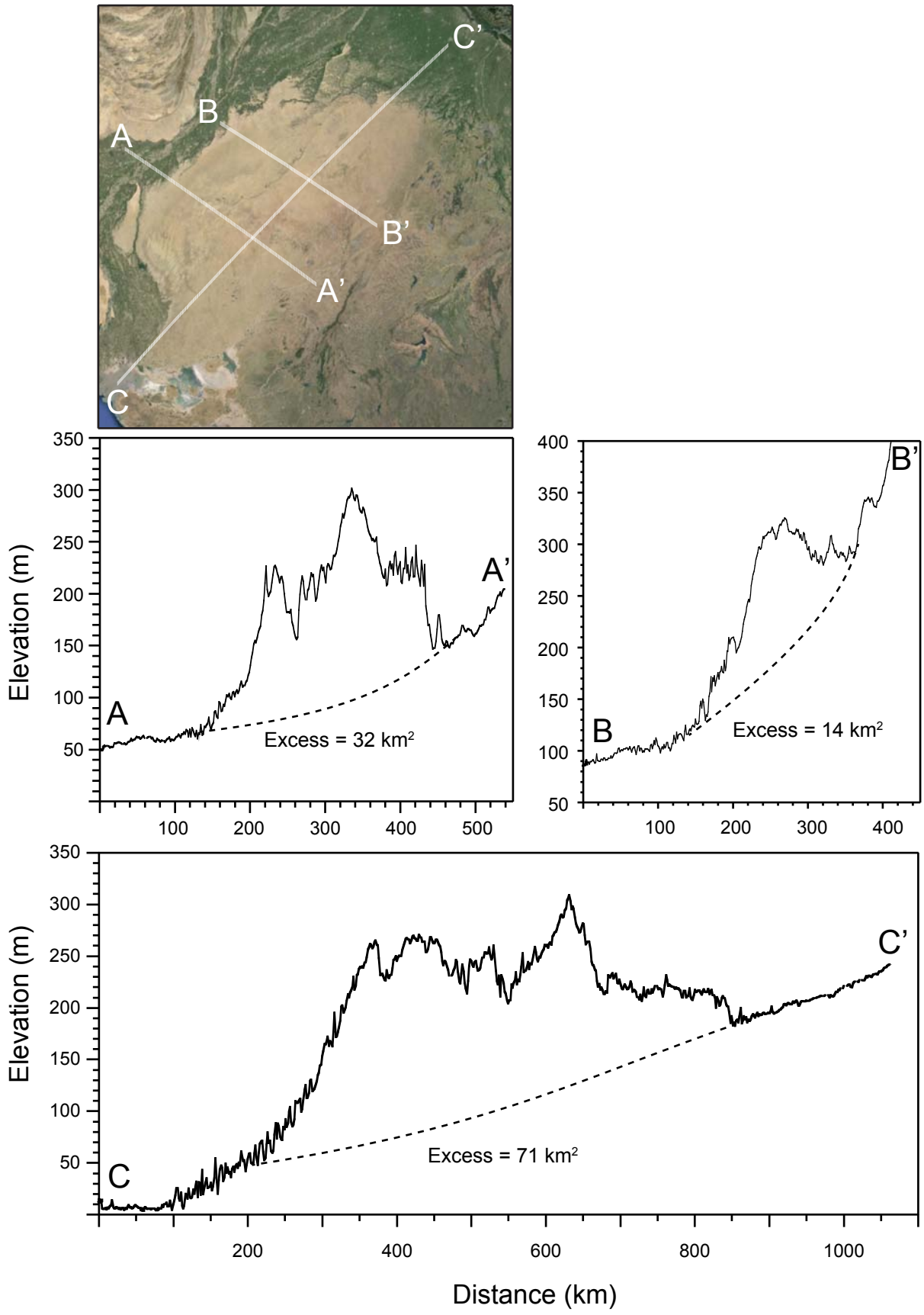

Figure 6
East et al.

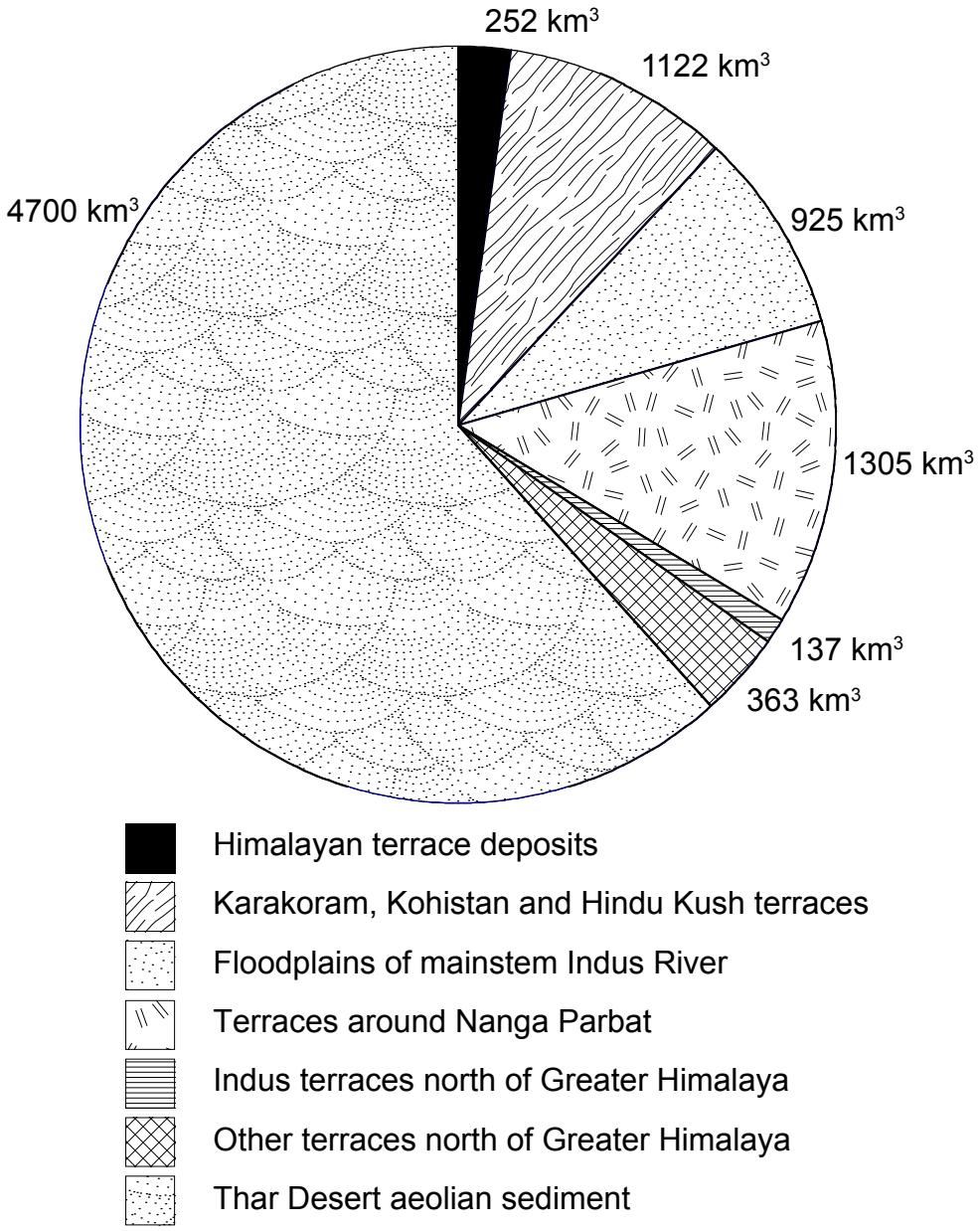

Figure 7
East et al.

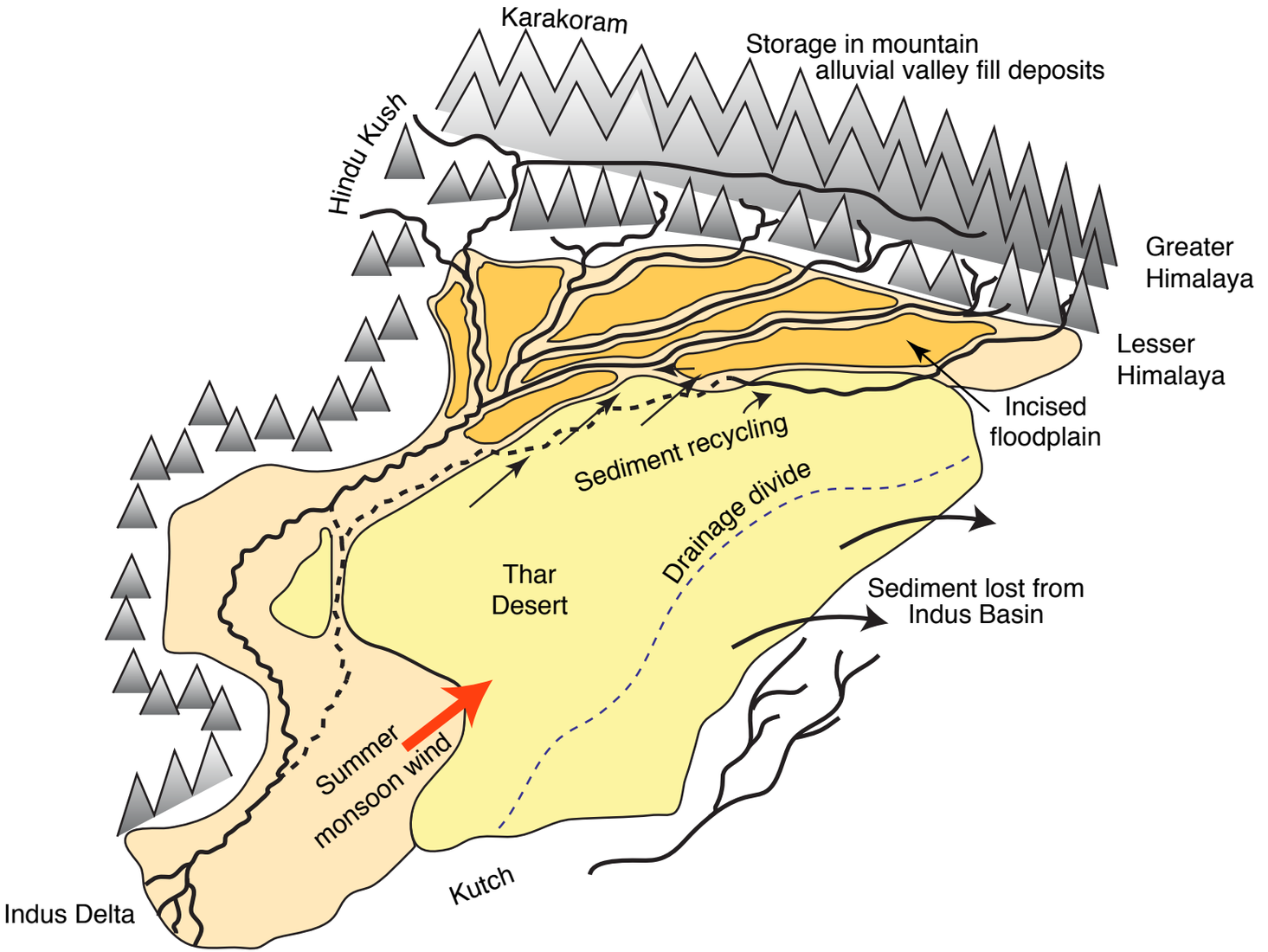
Karakoram
Storage in mountain
alluvial valley fill deposits
Hindu Kush
Greater
Himalaya
Lesser
Himalaya
Incised
floodplain
Sediment recycling
Drainage divide
Thar
Desert
Sediment lost from
Indus Basin
Summer
monsoon wind
Kutch
Indus Delta

Table 1. Sediment samples from which U-Pb zircon data are available for tracing provenance history among the Thar Desert, Indus River, and adjacent tributary basins (Sutlej River and Nara Valley).

Sample	Location	Latitude	Longitude	Sediment type	Data source
Thar Chak-310	Thar desert, downwind end	29.210867	72.484900	Aeolian dune	Alizai et al. (2011)
Thar UN1	Thar desert, upwind end, near Umerkot town	25.369611	69.732722	Aeolian dune	This study
Thar NM3	Thar desert, upwind end, near Mithi town	24.858972	69.726250	Aeolian dune	This study
Sutlej River	Sutlej River at Tatapani	31.000000	76.550000	Fluvial (modern)	Alizai et al. (2011a)
Nara	Nara Valley drill site (Nara-1), 15 m depth	26.976017	68.990900	Borehole sample, fluvial sand	This study
Indus River, modern	Modern Indus delta at Thatta	24.618817	68.049500	Fluvial (modern)	Clift et al. (2004)
Indus 7 ka TH-10	Indus delta at Thatta, 7 ka, 30 m depth	24.702306	67.990972	Borehole sample, fluvial sand	Clift et al. (2008)
Indus LGM KB-41-5	Indus delta at Keti Bandar	24.152400	67.515533	Fluvial (modern)	Clift et al. (2008)

Table 2. U-Pb zircon data for samples UN1, NM3, and Nara (see Table 1 for sample descriptions).

Sample UN1

Grain No.	Pb (ppm)	U (ppm)	Atomic Th/U	Ratios						Ages (Ma)						% discordant (206/238 207/235)	% discordant (206/238 207/206)	Best Age	±2σ
				206/238	± 1σ	207/235	± 1σ	207/206	± 1σ	206/238	± 2σ	207/235	± 2σ	207/206	± 2σ				
G1	13.7	94.5	2.10	0.0931	0.0013	0.7672	0.0299	0.0586	0.0019	574.1	15.8	578.1	30.2	553.8	26.9	0.7	-3.7	574.08	15.80
G2	97.3	300.5	0.63	0.2859	0.0036	3.7774	0.0766	0.0945	0.0013	1621.1	36.5	1587.9	30.3	1518.1	30.0	-2.1	-6.8	1518.13	29.99
G3	193.1	511.2	0.05	0.3788	0.0049	6.0808	0.1380	0.1188	0.0017	2070.7	45.4	1987.5	33.4	1937.5	32.5	-4.2	-6.9	1937.50	32.45
G4	76.2	848.1	0.65	0.0811	0.0010	0.6353	0.0123	0.0565	0.0009	502.8	12.4	499.4	16.2	472.9	20.2	-0.7	-6.3	502.80	12.40
G5	31.5	1820.4	0.18	0.0179	0.0003	0.1274	0.0037	0.0515	0.0014	114.4	3.2	121.8	7.1	262.4	20.7	6.1	56.4	114.37	3.17
G6	497.0	990.6	0.19	0.4708	0.0059	10.4741	0.1903	0.1554	0.0020	2486.8	52.1	2477.6	32.9	2406.2	31.1	-0.4	-3.4	2406.21	31.09
G7	38.8	395.0	0.14	0.1021	0.0014	0.8886	0.0256	0.0622	0.0014	626.5	16.1	645.6	25.3	680.3	30.8	3.0	7.9	626.53	16.14
G8	147.9	312.6	0.58	0.4161	0.0054	8.4828	0.2104	0.1473	0.0021	2242.7	49.0	2284.1	34.9	2315.2	33.8	1.8	3.1	2315.17	33.85
G9	58.8	566.5	0.57	0.0956	0.0012	0.7892	0.0164	0.0586	0.0010	588.7	14.5	590.7	18.8	553.4	22.4	0.3	-6.4	588.75	14.47
G10	99.5	150.6	0.89	0.5144	0.0068	11.9929	0.3654	0.1626	0.0024	2675.3	57.5	2603.9	37.0	2482.4	35.5	-2.7	-7.8	2482.36	35.48
G11	143.2	306.6	0.32	0.4357	0.0056	9.6346	0.2179	0.1575	0.0021	2331.1	50.1	2400.5	34.2	2428.8	32.9	2.9	4.0	2428.78	32.94
G12	0.7	75.6	0.56	0.0090	0.0003	0.0603	0.0087	0.0486	0.0070	57.9	3.3	59.5	16.9	126.6	42.1	2.7	54.3	57.89	3.32
G13	1.8	125.6	0.58	0.0135	0.0003	0.0857	0.0077	0.0467	0.0041	86.6	3.6	83.5	14.7	35.5	14.1	-3.7	-144.4	86.64	3.56
G14	44.3	576.0	0.38	0.0750	0.0010	0.5748	0.0131	0.0555	0.0011	466.1	11.8	461.1	17.1	431.6	21.4	-1.1	-8.0	466.09	11.75
G15	11.3	574.6	0.91	0.0165	0.0002	0.1081	0.0041	0.0471	0.0017	105.6	3.0	104.2	7.7	54.8	11.8	-1.3	-92.7	105.62	3.04
G16	390.6	2351.2	0.25	0.1656	0.0021	1.7124	0.0269	0.0741	0.0009	987.7	23.0	1013.2	22.8	1042.8	24.5	2.5	5.3	1042.83	24.53
G17	3.2	181.6	0.97	0.0150	0.0003	0.1018	0.0067	0.0477	0.0031	95.8	3.4	98.5	12.2	82.9	18.2	2.7	-15.5	95.79	3.43
G18	35.8	227.6	0.95	0.1310	0.0017	1.2096	0.0322	0.0655	0.0013	793.6	19.7	805.0	26.7	789.2	30.3	1.4	-0.6	793.57	19.72
G19	9.6	549.0	0.56	0.0162	0.0003	0.1096	0.0054	0.0490	0.0024	103.7	3.3	105.6	10.2	149.7	21.4	1.8	30.7	103.72	3.30
G20	97.0	3439.0	0.13	0.0297	0.0004	0.2028	0.0037	0.0490	0.0008	188.7	4.8	187.5	6.9	148.3	12.3	-0.6	-27.2	188.67	4.76
G21	67.5	958.8	0.11	0.0742	0.0010	0.5622	0.0112	0.0547	0.0009	461.3	11.4	453.0	15.4	399.2	19.1	-1.8	-15.6	461.29	11.40
G22	24.0	157.3	0.35	0.1485	0.0020	1.3631	0.0402	0.0664	0.0015	892.3	22.3	873.2	30.0	820.0	32.5	-2.2	-8.8	892.27	22.34
G23	78.7	272.8	0.28	0.2807	0.0037	4.3071	0.1198	0.1122	0.0019	1594.7	37.3	1694.7	35.5	1835.8	36.7	5.9	13.1	1835.84	36.73
G24	79.3	486.8	0.23	0.1629	0.0021	1.5900	0.0327	0.0704	0.0011	972.8	23.2	966.3	25.2	938.6	27.1	-0.7	-3.6	938.59	27.14
G25	2.7	203.9	0.80	0.0113	0.0003	0.0801	0.0071	0.0519	0.0046	72.7	3.3	78.2	13.9	281.9	51.3	7.1	74.2	72.69	3.31
G26	52.8	2956.8	0.08	0.0192	0.0003	0.1271	0.0026	0.0474	0.0009	122.3	3.2	121.5	5.1	69.9	10.5	-0.6	-74.9	122.28	3.16
G27	187.7	2490.9	0.12	0.0790	0.0010	0.6207	0.0104	0.0560	0.0008	490.0	11.9	490.3	14.5	450.8	18.1	0.1	-8.7	490.03	11.95
G28	19.0	147.9	0.67	0.1139	0.0016	1.0145	0.0334	0.0633	0.0016	695.2	18.2	711.2	29.4	718.3	34.3	2.2	3.2	695.18	18.17
G29	84.9	835.3	0.23	0.1031	0.0014	0.9434	0.0265	0.0667	0.0015	632.3	16.2	674.6	25.7	827.8	33.1	6.3	23.6	632.32	16.25
G30	5.7	548.3	0.62	0.0094	0.0002	0.0590	0.0030	0.0464	0.0023	60.2	1.9	58.2	6.1	18.5	9.8	-3.3	-226.1	60.19	1.92
G31	1.4	605.7	1.30	0.0018	0.0001	0.0116	0.0015	0.0465	0.0062	11.5	0.6	11.7	3.1	23.1	14.1	1.7	50.4	11.46	0.64
G32	7.0	1028.4	0.12	0.0072	0.0001	0.0475	0.0020	0.0471	0.0020	46.1	1.4	47.1	4.0	52.3	12.3	2.1	11.8	46.12	1.41
G33	3.9	177.6	0.67	0.0196	0.0003	0.1259	0.0079	0.0475	0.0029	124.9	4.3	120.4	14.6	73.9	16.6	-3.8	-69.0	124.94	4.30
G34	310.2	574.6	0.52	0.4696	0.0060	10.4649	0.1968	0.1608	0.0021	2481.8	52.3	2476.8	33.8	2463.7	32.3	-0.2	-0.7	2463.67	32.29
G35	60.7	260.6	0.85	0.1957	0.0026	2.0584	0.0499	0.0753	0.0013	1152.3	27.5	1135.1	29.7	1076.5	31.3	-1.5	-7.0	1076.52	31.25
G36	283.7	750.2	0.12	0.3776	0.0049	7.6316	0.1810	0.1419	0.0021	2065.0	45.7	2188.6	34.8	2250.5	34.3	5.6	8.2	2250.52	34.25
G37	18.1	1018.2	0.56	0.0164	0.0002	0.1065	0.0033	0.0467	0.0014	104.7	2.9	102.8	6.3	32.9	9.9	-1.8	-218.3	104.67	2.92
G38	34.7	71.6	2.34	0.2971	0.0041	4.2879	0.1507	0.1065	0.0021	1677.1	40.5	1691.0	40.2	1741.0	41.4	0.8	3.7	1741.04	41.43
G39	3.1	163.4	0.48	0.0170	0.0004	0.1181	0.0173	0.0484	0.0070	108.4	4.8	113.4	30.3	116.9	40.1	4.4	7.3	108.35	4.82
G40	64.6	1470.7	0.99	0.0359	0.0005	0.2715	0.0057	0.0540	0.0010	227.5	5.8	243.9	9.7	371.9	19.5	6.7	38.8	227.49	5.85
G41	15.6	872.4	0.69	0.0159	0.0002	0.1065	0.0035	0.0481	0.0015	101.4	2.8	102.7	6.7	102.7	14.2	1.3	1.2	101.44	2.79
G42	18.2	108.0	0.44	0.1589	0.0022	1.5908	0.0562	0.0720	0.0018	950.5	24.6	966.6	35.7	986.5	39.7	1.7	3.7	986.51	39.71
G43	79.0	746.1	0.19	0.1084	0.0014	0.9216	0.0233	0.0616	0.0013	663.2	16.6	663.2	23.6	661.6	27.7	0.0	-0.2	663.16	16.63
G44	14.6	850.1	0.48	0.0161	0.0002	0.1058	0.0034	0.0468	0.0015	103.2	2.9	102.1	6.5	38.5	10.3	-1.1	-167.9	103.21	2.92
G45	10.1	1019.6	0.67	0.0089	0.0001	0.0575	0.0024	0.0463	0.0019	57.1	1.7	56.8	4.7	10.7	8.9	-0.5	-434.6	57.06	1.66
G46	14.3	85.8	0.21	0.1680	0.0024	1.7017	0.0614	0.0744	0.0019	1001.2	25.9	1009.2	37.3	1053.2	41.3	0.8	4.9	1053.15	41.28
G47	48.4	439.6	0.93	0.0911	0.0012	0.7496	0.0178	0.0589	0.0012	562.3	14.1	568.0	20.3	564.5	24.9	1.0	0.4	562.28	14.06
G48	229.0	1599.6	0.04	0.1524	0.0019	1.5003	0.0263	0.0707	0.0010	914.3	21.7	930.5	23.2	948.5	25.6	1.7	3.6	948.46	25.60
G49	6.2	336.9	0.58	0.0165	0.0003	0.1189	0.0070	0.0537	0.0031	105.4	3.7	114.1	13.2	360.2	42.5	7.6	70.7	105.43	3.68
G50	8.2	680.6	0.00	0.0127	0.0002	0.0943	0.0043	0.0560	0.0025	81.4	2.5	91.5	8.6	454.0	40.8	11.1	82.1	81.35	2.55
G51	4.7	305.9	1.82	0.0104	0.0002	0.0743	0.0063	0.0521	0.0043	66.6	2.9	72.8	12.1	288.0	49.8	8.5	76.9	66.57	2.93
G52	150.2	306.6	0.40	0.4442	0.0057	9.7984	0.2086	0.1622	0.0023	2369.2	50.9	2416.0	35.5	2478.2	34.6	1.9	4.4	2478.20	34.63
G53	4.0	1520.6	0.43	0.0025	0.0000	0.0166	0.0009	0.0464	0.0026	16.2	0.5	16.7	1.9	15.9	9.8	2.8	-2.3	16.22	0.51
G54	35.9	445.7	0.20	0.0824	0.0011	0.6527	0.0161	0.0585	0.0012	510.4	13.0	510.1	19.9	549.3	25.5	-0.1	7.1	510.43	12.98

G55	88.6	432.8	0.68	0.1792	0.0023	1.8740	0.0406	0.0748	0.0012	1062.6	25.4	1071.9	27.7	1062.1	29.8	0.9	-0.1	1062.06	29.83
G56	23.1	3312.0	0.47	0.0066	0.0001	0.0440	0.0012	0.0473	0.0013	42.3	1.2	43.7	2.5	63.4	11.3	3.3	33.3	42.28	1.15
G57	125.7	391.0	0.53	0.3019	0.0039	4.8306	0.1016	0.1153	0.0017	1700.8	38.4	1790.2	33.3	1884.7	33.8	5.0	9.8	1884.73	33.84
G58	52.0	436.2	0.69	0.1050	0.0014	0.9424	0.0222	0.0653	0.0013	643.4	16.1	674.2	22.9	785.3	28.9	4.6	18.1	643.35	16.10
G59	5.0	1513.9	0.33	0.0033	0.0001	0.0218	0.0011	0.0470	0.0024	21.1	0.6	21.9	2.2	46.7	12.6	3.6	54.8	21.11	0.64
G60	19.7	2858.3	1.40	0.0051	0.0001	0.0353	0.0011	0.0495	0.0015	32.7	0.9	35.2	2.3	173.0	17.6	7.3	81.1	32.66	0.90
G61	98.1	318.0	0.24	0.3017	0.0039	4.5660	0.1002	0.1128	0.0018	1699.7	38.6	1743.1	33.9	1845.3	34.5	2.5	7.9	1845.33	34.52
G62	101.5	744.8	0.17	0.1392	0.0018	1.3281	0.0306	0.0682	0.0012	840.3	20.6	858.1	25.6	875.5	29.1	2.1	4.0	840.31	20.60
G63	58.7	139.8	0.28	0.3972	0.0053	7.8878	0.2597	0.1384	0.0025	2156.0	49.3	2218.3	40.1	2207.4	40.1	2.8	2.3	2207.41	40.11
G64	141.4	466.6	0.21	0.3001	0.0039	4.7023	0.1087	0.1154	0.0019	1691.6	38.7	1767.7	34.7	1885.7	35.5	4.3	10.3	1885.67	35.47
G65	71.0	187.0	0.37	0.3521	0.0046	5.6271	0.1422	0.1166	0.0019	1944.5	43.9	1920.3	36.3	1904.1	36.3	-1.3	-2.1	1904.13	36.31
G66	15.1	1655.7	1.20	0.0070	0.0001	0.0462	0.0016	0.0477	0.0016	45.2	1.3	45.8	3.3	81.9	13.3	1.4	44.9	45.16	1.28
G67	15.8	108.0	0.41	0.1390	0.0021	1.3807	0.0622	0.0713	0.0023	839.2	23.7	880.8	42.3	966.0	48.9	4.7	13.1	839.18	23.66
G68	149.7	435.5	0.47	0.3127	0.0040	4.4473	0.0980	0.1049	0.0017	1754.0	39.7	1721.2	34.0	1711.9	34.2	-1.9	-2.5	1711.86	34.18
G69	77.4	1120.9	0.06	0.0738	0.0010	0.5920	0.0124	0.0564	0.0010	459.2	11.5	472.2	16.3	469.3	21.3	2.7	2.1	459.25	11.53
G70	9.0	946.7	1.00	0.0078	0.0001	0.0509	0.0022	0.0472	0.0020	49.9	1.5	50.4	4.4	58.9	12.8	0.9	15.2	49.90	1.54
G71	34.9	257.9	2.22	0.0832	0.0012	0.6973	0.0284	0.0608	0.0021	515.0	14.6	537.2	30.7	631.1	39.7	4.1	18.4	515.02	14.64
G72	66.1	829.9	0.11	0.0832	0.0011	0.8146	0.0177	0.0713	0.0013	515.0	12.9	605.0	20.3	964.6	30.5	14.9	46.6	514.96	12.86
G73	15.7	362.6	0.38	0.0421	0.0006	0.3146	0.0113	0.0534	0.0017	266.0	7.4	277.7	16.9	344.1	26.8	4.2	22.7	266.02	7.42
G74	6.9	594.9	1.00	0.0096	0.0002	0.0648	0.0033	0.0487	0.0024	61.4	2.0	63.8	6.4	135.3	20.6	3.7	54.6	61.40	2.04
G75	63.2	203.2	0.44	0.2899	0.0038	4.6312	0.1264	0.1150	0.0021	1641.0	38.4	1754.9	37.3	1880.2	38.8	6.5	12.7	1880.20	38.80
G76	3.8	458.5	0.93	0.0068	0.0001	0.0447	0.0028	0.0474	0.0030	43.6	1.5	44.4	5.6	70.4	16.5	1.7	38.1	43.62	1.54
G77	4.4	1636.8	0.29	0.0027	0.0000	0.0183	0.0010	0.0485	0.0026	17.1	0.5	18.4	1.9	121.8	20.1	7.5	86.0	17.06	0.51
G78	154.8	501.0	0.38	0.2919	0.0038	4.6095	0.1090	0.1148	0.0019	1651.1	38.0	1751.0	35.6	1877.2	36.9	5.7	12.0	1877.22	36.89
G79	63.2	546.9	0.42	0.1089	0.0015	0.9990	0.0256	0.0661	0.0014	666.5	16.9	703.3	24.9	810.5	31.1	5.2	17.8	666.53	16.86
G80	296.8	4814.4	0.02	0.0671	0.0009	0.5407	0.0102	0.0567	0.0009	418.4	10.4	438.9	14.3	479.1	20.3	4.7	12.7	418.36	10.39
G81	9.1	60.8	0.62	0.1334	0.0020	1.2779	0.0595	0.0683	0.0024	807.0	23.0	835.9	42.7	876.5	48.6	3.5	7.9	807.01	22.98
G82	8.3	460.5	0.64	0.0160	0.0002	0.1052	0.0045	0.0485	0.0020	102.3	3.0	101.5	8.6	123.2	17.5	-0.8	17.0	102.33	3.05
G83	18.6	1216.8	0.37	0.0148	0.0002	0.1122	0.0040	0.0532	0.0018	94.9	2.8	108.0	7.5	338.6	27.8	12.1	72.0	94.90	2.79
G84	23.5	253.2	0.77	0.0801	0.0011	0.6223	0.0192	0.0581	0.0015	496.8	13.1	491.3	23.3	532.8	29.5	-1.1	6.7	496.84	13.13
G85	86.9	240.4	0.75	0.3064	0.0040	4.7559	0.1205	0.1134	0.0020	1723.2	39.8	1777.1	37.1	1854.9	38.2	3.0	7.1	1854.92	38.18
G86	7.2	611.8	0.54	0.0108	0.0002	0.0702	0.0033	0.0480	0.0022	69.5	2.2	68.9	6.6	96.8	16.4	-0.9	28.2	69.50	2.17
G87	15.7	622.6	2.00	0.0166	0.0003	0.1114	0.0067	0.0496	0.0029	106.1	3.7	107.3	12.5	175.4	26.6	1.1	39.5	106.07	3.68
G88	2.4	205.3	0.81	0.0099	0.0002	0.0652	0.0066	0.0473	0.0048	63.3	3.1	64.1	12.7	64.4	20.6	1.3	1.8	63.25	3.06
G89	48.8	262.0	1.13	0.1476	0.0020	1.3885	0.0394	0.0681	0.0015	887.3	22.2	884.1	30.4	871.3	33.8	-0.4	-1.8	887.27	22.25
G90	90.9	165.4	0.35	0.4979	0.0066	12.2871	0.3486	0.1829	0.0032	2604.9	56.7	2626.6	41.3	2679.7	41.0	0.8	2.8	2679.71	40.97
G91	41.5	212.7	0.84	0.1661	0.0022	1.6431	0.0485	0.0716	0.0016	990.5	24.8	986.9	32.9	974.3	36.0	-0.4	-1.7	974.31	35.99
G92	87.1	301.2	0.30	0.2807	0.0037	4.4437	0.1109	0.1148	0.0021	1595.0	37.1	1720.5	37.0	1876.1	38.8	7.3	15.0	1876.12	38.84
G93	51.9	2582.1	0.16	0.0209	0.0003	0.1392	0.0034	0.0479	0.0011	133.2	3.5	132.4	6.4	96.3	12.0	-0.6	-38.3	133.22	3.54
G94	10.7	590.8	0.56	0.0174	0.0003	0.1186	0.0057	0.0498	0.0023	111.3	3.5	113.8	10.5	183.3	23.4	2.2	39.3	111.33	3.55
G95	34.2	441.6	0.26	0.0780	0.0011	0.6121	0.0206	0.0576	0.0016	483.9	13.0	484.9	24.6	515.7	31.0	0.2	6.2	483.87	13.04
G96	31.1	1873.8	0.49	0.0156	0.0002	0.1081	0.0034	0.0486	0.0014	100.0	2.8	104.2	6.2	126.6	14.9	4.0	21.0	100.04	2.79
G97	110.3	270.8	0.45	0.3683	0.0049	5.7587	0.1618	0.1130	0.0021	2021.5	46.1	1940.2	39.9	1847.7	40.1	-4.2	-9.4	1847.73	40.07
G98	16.6	111.4	0.60	0.1343	0.0019	1.2616	0.0484	0.0681	0.0020	812.6	21.9	828.6	37.0	872.8	42.4	1.9	6.9	812.58	21.94
G99	91.7	1307.9	0.11	0.0740	0.0010	0.6074	0.0147	0.0577	0.0012	460.2	11.8	481.9	18.4	517.2	24.7	4.5	11.0	460.21	11.76
G100	42.2	2267.4	0.46	0.0177	0.0002	0.1242	0.0037	0.0500	0.0014	113.2	3.0	118.9	6.8	196.4	17.9	4.7	42.3	113.23	3.04
G101	280.9	745.5	0.68	0.3269	0.0043	5.0818	0.1136	0.1142	0.0020	1823.4	41.4	1833.1	37.1	1867.5	37.9	0.5	2.4	1867.46	37.90
G102	61.3	921.0	0.07	0.0717	0.0010	0.5975	0.0177	0.0600	0.0015	446.3	11.8	475.7	21.7	603.6	30.9	6.2	26.1	446.33	11.79
G103	40.3	251.2	0.56	0.1463	0.0020	1.3396	0.0387	0.0674	0.0015	880.4	22.3	863.0	30.9	849.9	34.1	-2.0	-3.6	880.36	22.27
G104	341.4	1029.7	0.35	0.3132	0.0041	4.9377	0.1059	0.1134	0.0020	1756.4	40.0	1808.7	36.6	1853.8	37.6	2.9	5.3	1853.81	37.59
G105	116.1	702.9	0.90	0.1377	0.0018	1.2870	0.0305	0.0671	0.0013	831.6	20.5	840.0	26.8	840.3	30.3	1.0	1.0	831.59	20.51
G106	64.0	642.8	0.17	0.1023	0.0014	0.8349	0.0207	0.0602	0.0013	628.0	15.8	616.3	22.9	610.1	27.0	-1.9	-2.9	628.05	15.79
G107	6.9	54.0	1.19	0.0992	0.0016	0.8105	0.0455	0.0616	0.0028	609.9	19.2	602.7	44.9	658.9	52.1	-1.2	7.4	609.89	19.24
G108	12.4	686.7	0.53	0.0168	0.0003	0.1116	0.0043	0.0487	0.0018	107.4	3.2	107.4	8.2	131.0	17.0	0.0	18.0	107.40	3.17
G109	62.0	665.1	0.27	0.0935	0.0013	0.7501	0.0195	0.0588	0.0013	575.9	14.7	568.3	22.4	558.6	26.7	-1.3	-3.1	575.91	14.74
G110	102.4	310.6	0.48	0.3036	0.0041	4.6128	0.1349	0.1122	0.0023	1708.9	40.4	1751.6	40.5	1835.4	42.2	2.4	6.9	1835.35	42.18
G111	110.9	605.7	0.57	0.1664	0.0022	1.6755	0.0402	0.0727	0.0014	992.4	24.2	999.3	29.9	1005.3	32.9	0.7	1.3	1005.32	32.92
G112	23.4	274.8	0.25	0.0859	0.0012	0.7161	0.0261	0.0608	0.0019	531.0	14.6	548.4	28.6	633.6	36.7	3.2	16.2	531.01	14.60
G113	43.5	139.8	0.80	0.2631	0.0036	3.5634	0.1245	0.0969	0.0022	1505.8	37.2	1541.4	42.3	1564.5	44.6	2.3	3.8	1564.51	44.56
G114	45.5	194.5	0.65	0.2064	0.0028	2.2882	0.0680	0.0811	0.0018	1209.6	29.8	1208.7	36.5	1223.9	39.2	-0.1	1.2	1223.87	39.20
G115	4.7	563.8	0.78	0.0072	0.0002	0.0527	0.0039	0.0522	0.0039	46.4	1.9	52.1	7.7	293.3	45.6	11.0	84.2	46.38	1.92
G116	16.2	534.1	0.78	0.0264	0.0004	0.1821	0.0064	0.0506	0.0017	168.0	4.8	169.8	11.3	220.8	20.9	1.1	23.9	168.04	4.77

G117	5.2	284.3	0.55	0.0169	0.0003	0.1124	0.0063	0.0472	0.0025	108.2	3.5	108.1	11.3	61.4	14.4	-0.1	-76.3	108.22	3.55
G118	53.5	394.3	0.54	0.1243	0.0017	1.1709	0.0348	0.0682	0.0016	755.0	19.4	787.1	30.1	874.3	36.0	4.1	13.6	755.04	19.38
G119	47.4	299.1	1.05	0.1281	0.0018	1.1766	0.0410	0.0672	0.0018	777.2	20.6	789.7	33.9	845.2	39.4	1.6	8.0	777.19	20.57

Sample NM3

				Ratios						Ages (Ma)									
Grain No.	Pb (ppm)	U (ppm)	Atomic Th/U	206/238	± 1σ	207/235	± 1σ	207/206	± 1σ	206/238	± 2σ	207/235	± 2σ	207/206	± 2σ	% discordant (206/238 207/235)	% discordant (206/238 207/206)	Best Age	±2σ
G1	319.9	2414.2	0.77	0.1167	0.0015	1.0220	0.0148	0.0633	0.0007	711.3	17.4	714.9	17.9	717.7	12.0	0.5	0.9	711.25	17.43
G2	82.3	252.4	0.49	0.2989	0.0039	4.6283	0.0764	0.1146	0.0013	1685.6	38.8	1754.4	29.4	1873.6	43.0	3.9	10.0	1873.60	42.99
G3	166.5	475.2	0.12	0.3484	0.0045	5.3509	0.0798	0.1120	0.0012	1927.0	42.9	1877.0	29.1	1832.0	41.8	-2.7	-5.2	1831.96	41.78
G4	195.5	616.2	0.22	0.3125	0.0041	4.8506	0.0757	0.1135	0.0013	1752.8	39.8	1793.7	29.1	1856.2	42.4	2.3	5.6	1856.19	42.37
G5	193.9	1185.3	0.02	0.1748	0.0022	1.7439	0.0246	0.0723	0.0008	1038.6	24.6	1024.9	22.0	995.2	37.2	-1.3	-4.4	995.24	37.20
G6	54.1	190.6	0.60	0.2538	0.0034	3.2246	0.0631	0.0919	0.0012	1457.8	34.9	1463.1	29.2	1465.9	43.6	0.4	0.6	1465.94	43.58
G7	10.4	568.3	0.56	0.0169	0.0002	0.1144	0.0027	0.0484	0.0011	108.0	3.0	109.9	5.5	120.3	28.2	1.7	10.2	108.03	3.04
G8	385.3	773.7	0.32	0.4588	0.0059	10.3036	0.1470	0.1631	0.0018	2434.2	51.9	2462.4	31.1	2487.8	43.1	1.1	2.2	2487.85	43.13
G9	1.3	159.3	0.30	0.0081	0.0002	0.0576	0.0046	0.0515	0.0042	51.7	2.9	56.9	9.5	261.9	60.8	9.0	80.2	51.75	2.94
G10	79.6	461.3	0.09	0.1805	0.0023	1.8581	0.0294	0.0745	0.0009	1069.9	25.6	1066.3	23.4	1055.6	38.8	-0.3	-1.4	1055.58	38.85
G11	691.2	1270.6	0.79	0.4543	0.0058	10.4268	0.1592	0.1646	0.0018	2414.4	51.7	2473.4	31.4	2503.9	43.5	2.4	3.6	2503.88	43.54
G12	149.7	423.0	0.59	0.3157	0.0041	4.8679	0.0762	0.1141	0.0013	1768.8	39.8	1796.7	29.0	1865.6	42.5	1.6	5.2	1865.56	42.45
G13	2.1	220.2	1.01	0.0080	0.0002	0.0595	0.0033	0.0558	0.0032	51.2	2.3	58.6	7.2	444.0	64.1	12.7	88.5	51.17	2.30
G14	153.1	440.4	0.70	0.3031	0.0040	4.7002	0.0831	0.1127	0.0014	1706.4	39.2	1767.3	29.8	1842.6	43.5	3.4	7.4	1842.60	43.52
G15	53.2	141.9	1.58	0.2714	0.0036	3.5782	0.0720	0.0937	0.0013	1548.1	36.7	1544.7	29.8	1502.5	43.9	-0.2	-3.0	1502.48	43.91
G16	198.5	16072.7	0.06	0.0133	0.0002	0.0911	0.0013	0.0480	0.0006	85.4	2.2	88.5	2.8	97.8	25.2	3.5	12.6	85.43	2.16
G17	109.6	483.9	0.53	0.2083	0.0028	2.4724	0.0519	0.0848	0.0012	1219.9	30.0	1264.0	28.5	1311.2	44.4	3.5	7.0	1311.20	44.35
G18	10.2	542.2	0.78	0.0164	0.0003	0.1236	0.0038	0.0539	0.0016	105.1	3.3	118.3	7.5	365.6	41.6	11.1	71.2	105.12	3.30
G19	1.9	180.2	1.01	0.0088	0.0002	0.0569	0.0035	0.0474	0.0029	56.3	2.4	56.2	7.2	68.4	31.2	-0.2	17.7	56.29	2.43
G20	61.2	360.3	0.19	0.1719	0.0023	1.7776	0.0353	0.0769	0.0011	1022.7	25.3	1037.3	25.9	1118.3	42.7	1.4	8.5	1118.34	42.74
G21	143.2	421.2	0.33	0.3239	0.0042	5.0340	0.0842	0.1132	0.0013	1808.6	40.7	1825.1	29.7	1850.9	43.2	0.9	2.3	1850.93	43.16
G22	11.1	105.3	1.10	0.0846	0.0013	0.6799	0.0220	0.0596	0.0016	523.6	15.7	526.7	25.7	588.4	46.8	0.6	11.0	523.64	15.69
G23	44.1	103.6	0.62	0.3730	0.0052	6.4933	0.1676	0.1287	0.0018	2043.5	48.8	2045.0	35.2	2080.7	48.3	0.1	1.8	2080.70	48.28
G24	169.2	418.6	0.14	0.4001	0.0053	8.8777	0.1723	0.1567	0.0019	2169.6	48.3	2325.5	32.5	2420.7	45.3	6.7	10.4	2420.68	45.34
G25	46.0	346.4	0.74	0.1160	0.0016	1.0416	0.0211	0.0665	0.0011	707.6	18.0	724.7	21.8	821.5	41.0	2.4	13.9	707.56	18.02
G26	248.2	889.4	0.13	0.2847	0.0036	4.4991	0.0702	0.1149	0.0013	1615.0	36.5	1730.8	28.7	1878.8	42.8	6.7	14.0	1878.79	42.80
G27	166.1	538.7	0.31	0.2974	0.0038	4.7010	0.0786	0.1137	0.0014	1678.4	38.1	1767.4	29.4	1859.5	43.4	5.0	9.7	1859.53	43.39
G28	6.9	356.0	0.84	0.0167	0.0003	0.1134	0.0035	0.0479	0.0015	106.9	3.3	109.1	6.9	92.8	28.4	2.0	-15.1	106.89	3.30
G29	34.5	146.2	1.12	0.1882	0.0025	2.1172	0.0442	0.0797	0.0012	1111.7	27.3	1154.4	27.3	1188.3	43.7	3.7	6.4	1188.33	43.75
G30	62.8	114.0	0.02	0.5557	0.0076	19.7320	0.5075	0.2459	0.0031	2848.9	63.0	3078.3	35.8	3158.4	47.3	7.5	9.8	3158.43	47.30
G31	71.7	343.8	0.97	0.1740	0.0023	1.7280	0.0297	0.0725	0.0010	1034.3	24.7	1019.0	23.7	998.9	39.7	-1.5	-3.5	998.89	39.67
G32	120.5	294.2	0.75	0.3492	0.0045	5.6943	0.0942	0.1187	0.0014	1930.6	42.7	1930.5	30.1	1936.3	43.4	0.0	0.3	1936.29	43.39
G33	18.4	140.1	0.65	0.1183	0.0018	1.1498	0.0333	0.0662	0.0015	720.8	20.2	777.1	27.9	811.8	47.5	7.3	11.2	720.77	20.18
G34	55.7	114.9	2.22	0.3036	0.0040	4.3667	0.0905	0.1046	0.0014	1709.1	39.9	1706.1	31.2	1707.6	45.1	-0.2	-0.1	1707.65	45.11
G35	533.3	1074.8	0.29	0.4603	0.0058	10.4955	0.1491	0.1618	0.0018	2440.7	51.0	2479.5	31.0	2474.6	43.6	1.6	1.4	2474.56	43.61
G36	3.0	154.9	1.06	0.0158	0.0003	0.1042	0.0058	0.0491	0.0027	100.7	4.3	100.6	11.7	151.2	38.7	-0.1	33.4	100.74	4.32
G37	4.0	960.8	0.68	0.0038	0.0001	0.0242	0.0010	0.0469	0.0020	24.2	0.9	24.2	2.2	44.1	26.6	0.2	45.2	24.19	0.90
G38	162.4	255.9	0.89	0.5094	0.0065	13.0548	0.2237	0.1877	0.0022	2654.0	55.6	2683.6	32.6	2722.5	45.0	1.1	2.5	2722.46	44.96
G39	131.8	423.0	0.22	0.3075	0.0039	4.7606	0.0787	0.1125	0.0014	1728.5	38.7	1778.0	29.4	1839.4	43.4	2.8	6.0	1839.38	43.39
G40	5.6	591.8	1.17	0.0074	0.0001	0.0499	0.0017	0.0493	0.0017	47.5	1.5	49.5	3.6	161.6	33.1	4.1	70.6	47.46	1.54
G41	113.3	604.9	0.79	0.1608	0.0020	1.5574	0.0245	0.0708	0.0009	961.3	22.7	953.4	22.0	951.1	38.3	-0.8	-1.1	951.07	38.35
G42	122.7	411.7	0.26	0.2909	0.0038	4.5186	0.0818	0.1130	0.0014	1645.8	37.6	1734.4	30.1	1848.4	44.5	5.1	11.0	1848.37	44.53
G43	81.5	241.9	0.40	0.3163	0.0043	5.0608	0.1158	0.1141	0.0016	1771.6	41.6	1829.6	32.9	1866.2	47.1	3.2	5.1	1866.19	47.08
G44	48.9	134.9	0.52	0.3273	0.0043	5.2458	0.1063	0.1150	0.0015	1825.0	41.7	1860.1	31.6	1880.0	45.5	1.9	2.9	1880.04	45.47
G45	11.6	761.5	0.11	0.0162	0.0002	0.1171	0.0034	0.0517	0.0015	103.3	3.0	112.4	6.7	272.2	36.4	8.1	62.0	103.34	3.05
G46	80.5	253.3	0.38	0.3006	0.0039	4.9600	0.0863	0.1190	0.0015	1694.4	38.3	1812.5	30.2	1941.6	44.5	6.5	12.7	1941.56	44.52
G47	17.5	1118.3	0.30	0.0155	0.0002	0.1141	0.0025	0.0533	0.0011	99.3	2.7	109.7	5.2	341.6	35.1	9.5	70.9	99.28	2.67
G48	1.7	122.7	0.60	0.0123	0.0003	0.0874	0.0057	0.0491	0.0032	79.1	3.7	85.1	10.9	154.5	41.8	7.1	48.8	79.06	3.69
G49	59.2	303.7	1.44	0.1443	0.0019	1.3657	0.0257	0.0681	0.0010	868.7	21.2	874.3	22.8	871.3	40.0	0.6	0.3	868.71	21.18

G50	163.6	2408.1	0.04	0.0733	0.0009	0.5962	0.0087	0.0572	0.0007	456.1	11.1	474.8	13.0	499.3	32.6	3.9	8.6	456.13	11.05
G51	18.1	327.2	1.21	0.0431	0.0006	0.3100	0.0072	0.0517	0.0011	272.3	7.4	274.1	12.0	270.4	32.9	0.7	-0.7	272.27	7.42
G52	25.8	1949.5	0.27	0.0133	0.0002	0.0968	0.0023	0.0504	0.0011	85.4	2.4	93.8	4.6	213.5	31.6	9.0	60.0	85.36	2.42
G53	168.2	323.8	1.12	0.4055	0.0051	8.3220	0.1395	0.1451	0.0018	2194.1	47.0	2266.7	31.6	2289.3	44.9	3.2	4.2	2289.32	44.91
G54	174.5	586.6	0.13	0.3016	0.0038	5.2043	0.0890	0.1224	0.0015	1699.0	37.9	1853.3	30.2	1991.1	44.7	8.3	14.7	1991.07	44.67
G55	261.8	3531.7	0.27	0.0744	0.0009	0.6076	0.0091	0.0564	0.0007	462.7	11.2	482.0	13.2	467.8	32.4	4.0	1.1	462.67	11.16
G56	2.5	177.5	0.89	0.0117	0.0002	0.0900	0.0044	0.0569	0.0028	74.9	2.9	87.5	9.0	488.0	60.9	14.5	84.7	74.86	2.93
G57	112.5	1512.6	0.06	0.0797	0.0010	0.6599	0.0101	0.0597	0.0008	494.2	11.9	514.5	14.5	593.8	34.6	3.9	16.8	494.21	11.94
G58	63.2	379.5	0.31	0.1635	0.0021	1.6881	0.0333	0.0729	0.0011	976.4	23.6	1004.0	25.0	1012.3	42.1	2.8	3.5	1012.29	42.14
G59	6.4	418.6	0.47	0.0145	0.0002	0.0991	0.0035	0.0494	0.0017	92.5	2.9	96.0	7.0	167.3	33.8	3.6	44.7	92.48	2.92
G60	3.9	43.5	0.45	0.0837	0.0015	0.7997	0.0363	0.0645	0.0024	517.9	18.2	596.7	35.6	757.1	62.2	13.2	31.6	517.87	18.20
G61	8.8	592.7	0.15	0.0156	0.0002	0.1064	0.0030	0.0496	0.0014	100.0	2.9	102.7	6.1	175.8	31.8	2.7	43.1	99.98	2.92
G62	151.9	254.1	1.81	0.4059	0.0052	9.0702	0.1827	0.1596	0.0021	2196.0	48.1	2345.1	33.5	2450.9	47.1	6.4	10.4	2450.90	47.10
G63	2.5	332.5	0.51	0.0070	0.0002	0.0465	0.0029	0.0474	0.0030	45.2	2.0	46.2	6.0	70.4	31.6	2.0	35.8	45.22	2.05
G64	120.0	409.9	0.19	0.2929	0.0037	4.9005	0.0874	0.1153	0.0015	1656.1	37.0	1802.3	30.4	1884.6	45.3	8.1	12.1	1884.58	45.29
G65	3.8	207.1	0.71	0.0165	0.0003	0.1085	0.0048	0.0480	0.0021	105.4	3.8	104.6	9.5	99.3	31.3	-0.8	-6.1	105.37	3.81
G66	37.3	219.3	0.99	0.1400	0.0020	1.4960	0.0386	0.0754	0.0014	844.4	22.1	928.8	28.5	1080.0	48.4	9.1	21.8	844.44	22.05
G67	14.6	1225.4	0.01	0.0131	0.0002	0.0887	0.0023	0.0479	0.0012	84.0	2.4	86.3	4.7	95.3	27.6	2.6	11.8	84.03	2.42
G68	6.6	515.2	3.40	0.0066	0.0001	0.0394	0.0016	0.0514	0.0021	42.6	1.5	39.3	4.1	259.3	42.0	-8.5	83.6	42.60	1.54
G69	60.3	95.7	1.28	0.4692	0.0061	11.1626	0.2439	0.1753	0.0024	2480.2	53.6	2536.8	35.0	2609.1	48.2	2.2	4.9	2609.09	48.24
G70	87.1	271.5	0.37	0.3051	0.0039	4.9605	0.1014	0.1166	0.0016	1716.4	38.9	1812.6	32.1	1904.4	47.0	5.3	9.9	1904.43	47.04
G71	11.4	718.9	0.34	0.0157	0.0002	0.1040	0.0026	0.0485	0.0012	100.5	2.8	100.4	5.4	121.8	28.5	-0.1	17.5	100.49	2.79
G72	4.8	270.7	0.71	0.0155	0.0003	0.1021	0.0044	0.0478	0.0020	98.8	3.4	98.7	8.5	88.4	30.1	-0.1	-11.8	98.84	3.43
G73	118.2	379.5	0.34	0.2982	0.0038	4.6744	0.0900	0.1126	0.0016	1682.5	37.8	1762.7	31.4	1841.0	46.4	4.5	8.6	1840.99	46.40
G74	21.8	791.1	0.70	0.0244	0.0003	0.1669	0.0035	0.0497	0.0010	155.2	4.0	156.8	6.8	180.5	29.4	1.0	14.0	155.22	4.03
G75	17.7	2056.5	1.34	0.0064	0.0001	0.0439	0.0011	0.0476	0.0012	41.0	1.2	43.6	2.4	78.9	26.9	6.0	48.1	41.00	1.15
G76	197.5	1477.8	0.36	0.1305	0.0016	1.2970	0.0220	0.0697	0.0010	790.5	18.7	844.4	21.2	918.6	39.8	6.4	13.9	790.55	18.70
G77	70.1	213.2	0.69	0.2889	0.0038	4.6926	0.1100	0.1140	0.0017	1636.2	38.3	1765.9	33.7	1863.3	49.1	7.3	12.2	1863.34	49.06
G78	278.3	670.1	0.27	0.3983	0.0050	8.3694	0.1534	0.1516	0.0020	2161.1	46.2	2271.9	33.3	2364.5	47.5	4.9	8.6	2364.50	47.53
G79	6.0	445.6	1.13	0.0109	0.0002	0.0805	0.0030	0.0536	0.0020	70.0	2.4	78.6	6.3	352.2	45.4	11.0	80.1	70.01	2.42
G80	52.1	68.8	1.72	0.5480	0.0072	19.5545	0.4807	0.2531	0.0035	2816.8	60.2	3069.6	37.0	3204.1	50.0	8.2	12.1	3204.14	50.04
G81	37.7	297.6	0.54	0.1181	0.0016	1.1422	0.0264	0.0680	0.0013	719.3	18.2	773.5	24.3	867.3	44.4	7.0	17.1	719.33	18.22
G82	69.5	406.4	0.54	0.1587	0.0021	1.6879	0.0349	0.0755	0.0012	949.4	22.8	1004.0	26.0	1082.9	44.3	5.4	12.3	1082.91	44.33
G83	106.7	231.5	1.86	0.3081	0.0040	5.0607	0.1059	0.1196	0.0018	1731.4	39.1	1829.5	33.1	1949.7	48.4	5.4	11.2	1949.66	48.36
G84	8.6	50.5	0.76	0.1474	0.0024	1.6109	0.0607	0.0786	0.0021	886.1	26.6	974.5	39.1	1163.1	60.2	9.1	23.8	886.15	26.63
G85	12.3	126.2	1.04	0.0797	0.0011	0.6394	0.0182	0.0571	0.0014	494.5	13.6	502.0	21.9	494.6	41.8	1.5	0.0	494.45	13.61
G86	7.0	256.7	0.88	0.0231	0.0004	0.1559	0.0056	0.0483	0.0017	147.0	4.7	147.1	10.4	113.5	30.5	0.1	-29.5	147.03	4.66
G87	302.9	606.6	0.45	0.4569	0.0057	12.0837	0.2077	0.1879	0.0026	2425.6	50.0	2610.9	34.4	2723.4	48.7	7.1	10.9	2723.43	48.68
G88	457.9	3519.5	0.10	0.1367	0.0017	1.4197	0.0231	0.0724	0.0010	825.7	19.1	897.2	21.8	998.3	40.7	8.0	17.3	825.75	19.06
G89	74.8	409.9	2.16	0.1170	0.0015	1.0707	0.0233	0.0672	0.0012	713.4	17.7	739.1	23.3	842.4	43.3	3.5	15.3	713.39	17.66
G90	17.1	1826.8	0.69	0.0084	0.0001	0.0568	0.0015	0.0472	0.0012	53.7	1.5	56.1	3.0	59.9	25.9	4.3	10.3	53.67	1.53
G91	69.3	525.7	0.35	0.1283	0.0016	1.2815	0.0258	0.0706	0.0012	778.1	18.7	837.5	23.5	946.1	43.2	7.1	17.8	778.10	18.74
G92	4.5	2052.2	0.12	0.0023	0.0000	0.0153	0.0007	0.0466	0.0020	14.8	0.5	15.4	1.4	26.2	25.3	3.6	43.5	14.81	0.51
G93	10.0	1287.2	0.07	0.0084	0.0001	0.0569	0.0017	0.0475	0.0014	53.6	1.5	56.2	3.4	73.4	27.1	4.6	27.0	53.60	1.53
G94	26.8	1973.8	0.16	0.0141	0.0002	0.1024	0.0025	0.0502	0.0012	90.3	2.4	99.0	4.8	202.4	31.5	8.8	55.4	90.26	2.42
G95	1.4	279.4	0.64	0.0070	0.0001	0.0510	0.0026	0.0530	0.0027	44.7	1.8	50.5	5.4	328.4	51.5	11.5	86.4	44.71	1.79
G96	1.8	119.2	0.85	0.0131	0.0003	0.0858	0.0056	0.0479	0.0031	83.7	3.8	83.6	11.2	93.3	34.7	-0.2	10.3	83.71	3.82
G97	11.6	1384.6	1.19	0.0066	0.0001	0.0459	0.0014	0.0494	0.0015	42.2	1.3	45.6	2.9	166.9	32.1	7.5	74.7	42.15	1.28
G98	22.5	1595.3	0.43	0.0136	0.0002	0.0968	0.0023	0.0485	0.0011	86.8	2.3	93.8	4.5	121.3	28.2	7.4	28.4	86.83	2.29
G99	94.7	243.9	0.68	0.3369	0.0044	5.2618	0.1212	0.1161	0.0017	1871.5	42.0	1862.7	33.9	1897.3	25.7	-0.5	1.4	1897.33	25.73
G100	12.5	522.6	0.93	0.0199	0.0003	0.1324	0.0069	0.0487	0.0024	126.8	4.0	126.2	12.6	134.4	18.2	-0.5	5.6	126.83	4.05
G101	50.1	210.4	0.93	0.1978	0.0026	2.0830	0.0566	0.0776	0.0015	1163.4	28.2	1143.2	32.2	1136.4	31.9	-1.8	-2.4	1136.39	31.88
G102	91.5	274.1	0.45	0.3097	0.0040	4.8898	0.1146	0.1171	0.0018	1739.4	39.5	1800.5	34.1	1912.9	32.2	3.4	9.1	1912.89	32.22
G103	73.5	386.0	0.27	0.1885	0.0025	1.9700	0.0448	0.0779	0.0013	1113.2	26.6	1105.3	29.0	1144.8	28.9	-0.7	2.8	1144.83	28.87
G104	1.4	155.5	1.11	0.0070	0.0002	0.0474	0.0061	0.0484	0.0062	44.8	2.4	47.0	11.8	118.4	34.3	4.7	62.2	44.78	2.43
G105	2.6	138.8	1.40	0.0137	0.0003	0.0935	0.0088	0.0501	0.0047	88.0	3.9	90.7	16.9	199.2	39.3	3.0	55.8	87.97	3.94
G106	1.3	90.6	0.85	0.0121	0.0004	0.0807	0.0130	0.0496	0.0079	77.8	5.1	78.8	25.4	173.9	56.8	1.3	55.3	77.79	5.10
G107	101.6	334.6	0.19	0.3002	0.0039	4.1188	0.0963	0.1033	0.0017	1692.4	38.5	1658.0	34.1	1684.1	32.2	-2.1	-0.5	1684.06	32.19
G108	115.7	1139.1	0.27	0.1019	0.0013	0.8796	0.0198	0.0629	0.0012	625.3	15.4	640.8	21.6	706.2	24.5	2.4	11.5	625.30	15.45
G109	296.7	576.3	0.33	0.4729	0.0060	11.1222	0.2239	0.1739	0.0026	2496.3	52.8	2533.4	36.3	2595.9	33.1	1.5	3.8	2595.92	33.07
G110	4.9	292.0	0.28	0.0170	0.0003	0.1065	0.0061	0.0476	0.0027	108.4	3.5	102.7	11.8	76.9	13.9	-5.5	-40.8	108.35	3.55
G111	216.8	693.8	1.14	0.2470	0.0032	3.0659	0.0699	0.0923	0.0016	1422.9	33.0	1424.2	32.6	1472.7	31.7	0.1	3.4	1472.74	31.73

G112	42.0	536.0	0.12	0.0824	0.0011	0.8036	0.0247	0.0674	0.0017	510.4	13.5	598.8	25.2	848.9	34.5	14.8	39.9	510.43	13.46
G113	22.9	2025.3	0.61	0.0102	0.0001	0.0698	0.0023	0.0488	0.0015	65.4	1.8	68.5	4.5	137.3	13.7	4.5	52.3	65.42	1.79
G114	13.7	475.6	0.17	0.0300	0.0005	0.2115	0.0104	0.0536	0.0025	190.4	6.0	194.8	18.0	355.5	33.2	2.3	46.5	190.36	6.01
G115	10.5	617.7	0.47	0.0161	0.0002	0.1085	0.0048	0.0498	0.0021	102.8	3.0	104.6	9.1	183.8	19.9	1.7	44.1	102.83	3.05
G116	210.7	1358.4	0.89	0.1319	0.0017	1.1980	0.0279	0.0672	0.0013	798.8	19.5	799.7	25.6	842.4	27.3	0.1	5.2	798.75	19.48
G117	2.0	691.5	0.51	0.0027	0.0001	0.0174	0.0020	0.0476	0.0056	17.4	0.9	17.5	4.2	80.4	23.6	0.7	78.4	17.38	0.90
G118	186.2	1077.6	0.75	0.1506	0.0020	1.5447	0.0373	0.0735	0.0014	904.3	22.0	948.4	28.6	1028.9	30.6	4.6	12.1	1028.87	30.59
G119	12.9	989.2	0.99	0.0106	0.0002	0.0701	0.0031	0.0488	0.0021	68.2	2.0	68.8	6.1	139.7	16.7	0.9	51.2	68.23	2.04
G120	346.2	806.8	0.31	0.4071	0.0053	8.7244	0.2122	0.1604	0.0028	2201.6	48.2	2309.6	39.7	2459.6	37.9	4.7	10.5	2459.57	37.92
G121	155.6	430.8	0.81	0.3055	0.0040	4.9856	0.1220	0.1204	0.0022	1718.6	39.1	1816.9	37.9	1962.3	37.2	5.4	12.4	1962.31	37.20
G122	149.9	2054.4	0.16	0.0760	0.0010	0.6137	0.0154	0.0592	0.0013	472.0	12.0	485.9	19.7	574.8	24.6	2.8	17.9	472.02	11.98
G123	13.6	1300.2	0.66	0.0094	0.0002	0.0673	0.0037	0.0511	0.0028	60.6	2.0	66.2	7.2	243.1	29.0	8.5	75.1	60.57	2.04
G124	183.9	383.8	0.27	0.4513	0.0059	10.3326	0.2617	0.1685	0.0031	2401.0	52.0	2465.0	41.5	2543.1	39.7	2.6	5.6	2543.10	39.69
G125	9.3	2590.4	0.34	0.0035	0.0001	0.0242	0.0013	0.0492	0.0027	22.6	0.8	24.3	2.7	155.5	21.5	7.0	85.5	22.59	0.77
G126	28.9	296.5	0.62	0.0881	0.0012	0.7202	0.0251	0.0603	0.0018	544.1	14.5	550.8	27.9	614.0	32.7	1.2	11.4	544.05	14.46
G127	16.1	1312.5	0.86	0.0104	0.0002	0.0718	0.0039	0.0492	0.0026	66.5	2.2	70.4	7.5	156.9	21.2	5.6	57.6	66.51	2.17
G128	165.6	494.6	0.12	0.3377	0.0045	6.1833	0.1837	0.1344	0.0028	1875.6	43.1	2002.1	43.7	2155.7	43.4	6.3	13.0	2155.72	43.40
G129	186.8	356.9	0.45	0.4627	0.0062	9.9896	0.3391	0.1557	0.0034	2451.6	54.6	2433.8	47.3	2409.9	45.8	-0.7	-1.7	2409.93	45.82
G130	206.1	640.0	0.42	0.3009	0.0040	5.0362	0.1579	0.1214	0.0028	1695.9	39.8	1825.4	44.7	1976.3	45.2	7.1	14.2	1976.32	45.20
G131	225.8	284.2	0.96	0.6539	0.0086	27.8239	0.8640	0.3019	0.0065	3243.2	67.1	3412.9	49.4	3479.8	47.9	5.0	6.8	3479.85	47.85
G132	144.3	322.3	0.79	0.3760	0.0050	6.9169	0.2198	0.1375	0.0032	2057.5	46.9	2100.8	47.3	2196.5	46.9	2.1	6.3	2196.46	46.91
G133	195.5	306.6	0.45	0.5524	0.0073	13.6707	0.4350	0.2047	0.0047	2835.0	61.0	2727.2	50.4	2864.1	49.2	-4.0	1.0	2864.12	49.18
G134	73.7	979.1	0.24	0.0758	0.0010	0.6260	0.0205	0.0603	0.0017	470.7	12.3	493.6	24.7	614.0	31.7	4.6	23.3	470.70	12.34
G135	306.7	956.7	0.34	0.3070	0.0040	5.2002	0.1432	0.1249	0.0029	1726.1	39.7	1852.6	45.3	2027.2	46.1	6.8	14.9	2027.24	46.08
G136	4.6	436.4	1.41	0.0079	0.0002	0.0539	0.0052	0.0495	0.0048	50.5	2.3	53.3	10.2	169.2	35.6	5.2	70.2	50.47	2.30

Sample Nara

				Ratios						Ages (Ma)									
Grain No.	**Pb (ppm)**	**U (ppm)**	**Atomic Th/U**	**206/238**	**± s.e.**	**207/235**	**± s.e.**	**207/206**	**± s.e.**	**206/238**	**± 2σ**	**207/235**	**± 2σ**	**207/206**	**± 2σ**	**% concord. (206/238 207/235)**	**% concord. (206/238 207/206)**	**Best Age**	**±2s**
G84	7	2826	0.33	0.0026	0.0000	0.0172	0.0009			16.4	3.6	17.3	4.9	84.9	11.1	4.9	80.7	16.4	3.6
G49	3	620	1.8793	0.00375	0.0017	0.02479	0.0389			24.13	40.58	24.86	41.49	147.4	24.8	3.0	83.6	24.13	40.58
G92	4	906	0.02	0.0048	0.0001	0.0295	0.0020			30.6	4.4	29.5	7.5	43.1	8.9	-3.8	29.0	30.6	4.4
G36	8	1017	1.0124	0.00691	0.0001	0.04755	0.0016			44.39	20.67	47.17	21.43	244.9	26.5	5.9	81.9	44.39	20.67
G17	5	579	0.9290	0.00717	0.0023	0.04578	0.0453			46.06	48.32	45.45	47.91	55.3	20.8	-1.3	16.7	46.06	48.32
G44	2	234	0.8526	0.00736	0.0021	0.04639	0.0525			47.27	46.01	46.04	46.36	123.7	23.2	-2.7	61.8	47.27	46.01
G62	21	2235	1.38	0.0074	0.0001	0.0492	0.0018			47.5	4.4	48.8	6.7	100.7	9.8	2.5	52.8	47.5	4.4
G94	14	1942	0.16	0.0078	0.0001	0.0514	0.0019			50.2	4.5	50.9	6.8	54.8	6.8	1.3	8.4	50.2	4.5
G38	1	130	0.9568	0.00785	6E-05	0.04746	0.0008			50.41	20.03	47.08	21.25	122.3	23.4	-7.1	58.8	50.41	20.03
G16	2	236	1.0083	0.00789	0.002	0.0512	0.038			50.66	44.72	50.70	44.83	108.1	22.9	0.1	53.1	50.66	44.72
G13	2	187	0.7009	0.00801	0.0011	0.05153	0.0193			51.43	33.33	51.02	33.47	118.9	21.9	-0.8	56.7	51.43	33.33
G70	6	677	0.63	0.0082	0.0002	0.0557	0.0034			52.5	5.2	55.0	10.4	324.9	37.1	4.6	83.9	52.5	5.2
G53	5	533	1.1068	0.00839	0.0002	0.0552	0.0022			53.86	21.31	54.56	22.17	139.2	24.2	1.3	61.3	53.86	21.31
G27	6	625	0.4695	0.00867	0.0007	0.05567	0.0138			55.65	27.70	55.01	27.97	62.4	22.3	-1.2	10.8	55.65	27.70
G88	15	1699	0.22	0.0091	0.0001	0.0587	0.0020			58.3	4.7	57.9	7.0	19.5	4.4	-0.6	-199.0	58.3	4.7
G98	28	3057	0.33	0.0091	0.0036	0.0594	0.1108			58.7	49.5	58.6	48.6	56.8	7.7	-0.1	-3.2	58.7	49.5
G58	11	1031	0.2865	0.01039	0.0072	0.06784	0.6992			66.63	111.01	66.65	###	78.4	125.1	0.0	15.0	66.63	111.01
G93	4	381	0.39	0.0109	0.0003	0.0721	0.0057			70.1	6.7	70.7	16.2	415.1	57.7	0.9	83.1	70.1	6.7
G39	1	92	0.8110	0.01213	0.0001	0.07233	0.0015			77.72	20.92	70.91	21.91	144.0	22.9	-9.6	46.0	77.72	20.92
G7	1	64	0.6708	0.01219	0.0002	0.07291	0.0048			78.11	21.94	71.46	27.97	61.4	25.9	-9.3	-27.3	78.11	21.94
G41	3	206	0.5456	0.01243	0.0023	0.08087	0.0609			79.64	48.93	78.96	48.96	155.9	24.0	-0.9	48.9	79.64	48.93
G34	7	525	0.5720	0.01273	0.0008	0.0869	0.0167			81.54	29.45	84.61	30.72	216.2	30.7	3.6	62.3	81.54	29.45
G46	4	218	1.1419	0.01347	0.001	0.08948	0.0162			86.25	32.49	87.02	32.59	166.4	22.9	0.9	48.2	86.25	32.49
G50	4	243	0.6581	0.01384	0.0025	0.09055	0.0471			88.61	50.42	88.02	50.59	186.1	24.7	-0.7	52.4	88.61	50.42
G79	45	3262	0.19	0.0143	0.0002	0.0973	0.0025			91.7	5.3	94.3	7.5	93.3	7.0	2.8	1.8	91.7	5.3
G6	1	47	0.3706	0.01445	0.0004	0.09082	0.0032			92.48	23.84	88.27	24.33	327.5	23.7	-4.8	71.8	92.48	23.84
G31	1	87	0.6500	0.0146	0.0013	0.10196	0.0201			93.44	35.40	98.58	37.44	474.4	26.9	5.2	80.3	93.44	35.40

G91	20	1325	0.33	0.0152	0.0002	0.1018	0.0034	97.5	5.7	98.4	9.4	165.9	12.4	0.9	41.2	97.5	5.7
G37	9	572	0.5412	0.01569	0.0032	0.10357	0.094	100.36	60.39	100.07	59.84	160.7	25.1	-0.3	37.5	100.36	60.39
G3	1	92	0.3408	0.01573	9E-05	0.09645	0.0018	100.61	20.40	93.49	25.46	130.5	27.0	-7.6	22.9	100.61	20.40
G101	12	695	0.698	0.0159	0.0003	0.1182	0.0078	101.7	23.4	113.4	38.3	427.2	77.8	10.3	76.2	101.7	23.4
G43	13	767	0.5556	0.01597	0.0001	0.11628	0.0017	102.14	21.04	111.69	22.77	375.6	27.8	8.6	72.8	102.14	21.04
G73	46	2628	0.73	0.0160	0.0002	0.1074	0.0028	102.3	5.5	103.5	8.1	132.9	8.7	1.2	23.1	102.3	5.5
G78	59	3602	0.44	0.0162	0.0002	0.1122	0.0025	103.7	5.4	108.0	7.4	147.8	8.1	3.9	29.8	103.7	5.4
G25	22	1353	0.2482	0.01649	0.0035	0.10886	0.1136	105.43	63.27	104.92	61.71	110.6	23.8	-0.5	4.6	105.43	63.27
G52	7	345	0.9532	0.01662	0.0001	0.10914	0.0021	106.26	21.04	105.18	24.14	188.5	26.8	-1.0	43.6	106.26	21.04
G57	8	442	0.8019	0.01685	0.0008	0.12004	0.0094	107.72	29.02	115.11	29.76	350.9	25.1	6.4	69.3	107.72	29.02
G10	17	987	0.3555	0.01704	0.0009	0.11227	0.0134	108.92	31.05	108.04	30.69	96.3	21.2	-0.8	-13.1	108.92	31.05
G8	5	274	0.3933	0.01712	0.0029	0.11141	0.1135	109.43	55.64	107.25	54.63	138.2	24.0	-2.0	20.8	109.43	55.64
G5	3	141	0.6603	0.01743	0.0002	0.11128	0.0043	111.39	21.92	107.14	28.37	145.0	30.3	-4.0	23.2	111.39	21.92
G89	14	774	0.31	0.0176	0.0002	0.1102	0.0039	112.6	6.2	106.1	10.6	61.4	7.0	-6.1	-83.5	112.6	6.2
G65	37	2072	0.40	0.0178	0.0002	0.1184	0.0032	114.0	5.8	113.6	8.8	124.7	8.6	-0.4	8.6	114.0	5.8
G83	11	619	0.35	0.0179	0.0003	0.1159	0.0044	114.5	6.4	111.4	11.7	188.0	15.4	-2.8	39.1	114.5	6.4
G80	33	1496	0.02	0.0240	0.0003	0.1577	0.0046	153.0	6.9	148.7	11.2	126.6	9.3	-2.9	-20.8	153.0	6.9
G18	4	72	1.4473	0.04658	0.0001	0.31068	0.002	293.49	20.49	274.71	37.28	289.8	37.1	-6.8	-1.3	293.49	20.49
G22	14	223	0.5171	0.05799	0.001	0.42109	0.0155	363.39	31.57	356.83	31.60	386.8	25.6	-1.8	6.1	363.39	31.57
G51	66	1143	0.0575	0.0622	4E-05	0.48784	0.0008	388.99	19.75	403.44	37.40	490.0	40.4	3.6	20.6	388.99	19.75
G42	68	1089	0.0754	0.06642	0.0001	0.51293	0.0021	414.55	20.83	420.42	34.19	509.2	36.3	1.4	18.6	414.55	20.83
G85	19	232	1.14	0.0676	0.0009	0.4600	0.0159	421.4	14.4	384.2	26.4	542.9	27.9	-9.7	22.4	421.4	14.4
G33	26	294	1.1432	0.07123	0.0007	0.56937	0.0071	443.56	27.32	457.61	28.40	607.2	26.3	3.1	26.9	443.56	27.32
G74	174	2534	0.12	0.0726	0.0008	0.5783	0.0109	451.6	12.3	463.4	15.0	501.9	12.8	2.6	10.0	451.6	12.3
G30	44	561	0.5580	0.07353	0.0022	0.57128	0.0509	457.39	46.16	458.84	44.68	471.3	31.3	0.3	2.9	457.39	46.16
G86	292	4202	0.10	0.0739	0.0008	0.5837	0.0112	459.4	12.5	466.8	15.5	442.0	12.5	1.6	-3.9	459.4	12.5
G26	72	896	0.6831	0.07394	0.0001	0.58089	0.0012	459.85	20.82	465.03	25.91	515.7	26.3	1.1	10.8	459.85	20.82
G32	80	594	2.3443	0.08666	0.0006	0.69652	0.0061	535.75	26.02	536.71	27.83	556.4	26.0	0.2	3.7	535.75	26.02
G60	123	1406	0.20	0.0902	0.0010	0.7340	0.0158	556.8	14.8	558.9	19.0	574.5	16.2	0.4	3.1	556.8	14.8
G24	59	641	0.2276	0.09365	0.0005	0.77889	0.0064	577.09	24.68	584.85	29.24	633.6	28.7	1.3	8.9	577.09	24.68
G56	75	496	2.5731	0.09447	0.0025	0.76456	0.0576	581.92	48.59	576.64	45.96	596.3	32.2	-0.9	2.4	581.92	48.59
G81	60	572	0.26	0.1067	0.0012	0.8471	0.0194	653.3	17.0	623.0	22.4	679.6	19.4	-4.9	3.9	653.3	17.0
G67	349	2831	0.48	0.1189	0.0012	1.1973	0.0218	724.4	17.4	799.3	19.4	957.7	16.4	9.4	24.4	724.4	17.4
G1	138	1217	0.2630	0.11368	0.0035	1.04199	0.1623	694.08	60.01	724.91	54.84	790.1	36.2	4.3	12.2	724.91	54.84
G61	115	969	0.25	0.1195	0.0013	1.0443	0.0220	727.8	18.1	726.0	21.7	804.8	18.5	-0.2	9.6	727.8	18.1
G21	55	344	1.3983	0.12374	0.0001	1.08767	0.0029	752.05	20.64	747.37	56.94	787.2	57.8	-0.6	4.5	752.05	20.64
G9	45	313	0.7954	0.12538	0.0002	1.12948	0.0025	761.46	21.09	767.51	35.27	836.2	35.9	0.8	8.9	761.46	21.09
G4	22	159	0.5557	0.12633	0.0022	1.08617	0.0484	766.89	43.99	746.64	41.00	747.6	30.8	-2.7	-2.6	766.89	43.99
G90	242	1926	0.14	0.1306	0.0014	1.1832	0.0240	791.5	19.2	792.8	22.6	787.6	18.5	0.2	-0.5	791.5	19.2
G45	104	802	0.2479	0.13092	0.0001	1.26118	0.0019	793.11	20.86	828.44	31.85	958.0	32.9	4.3	17.2	793.11	20.86
G20	64	369	1.5085	0.13179	0.0015	1.1668	0.0283	798.07	35.78	785.15	35.17	803.8	29.5	-1.6	0.7	798.07	35.78
G14	175	1132	0.9253	0.13281	0.0001	1.24348	0.0022	803.88	20.51	820.46	53.21	834.0	53.8	2.0	3.6	803.88	20.51
G64	105	652	0.93	0.1390	0.0015	1.1731	0.0251	838.8	20.3	788.1	23.3	828.1	18.9	-6.4	-1.3	838.8	20.3
G11	23	154	0.4505	0.14447	0.0001	1.28824	0.0012	869.89	20.73	840.52	27.93	861.5	27.8	-3.5	-1.0	869.89	20.73
G87	45	286	0.49	0.1483	0.0019	1.2071	0.0356	891.5	23.9	803.8	32.6	861.2	28.3	-10.9	-3.5	891.5	23.9
G47	103	665	0.4258	0.1493	0.0021	1.45065	0.0699	897.04	43.04	910.14	49.21	968.6	44.6	1.4	7.4	897.04	43.04
G95	845	5797	0.02	0.1559	0.0017	1.5131	0.0303	934.0	21.8	935.7	24.7	898.4	20.1	0.2	-4.0	934.0	21.8
G63	528	3506	0.06	0.1596	0.0016	1.6162	0.0275	954.4	21.2	976.5	20.2	966.6	14.7	2.3	1.3	954.4	21.2
G55	14	78	0.8692	0.16063	8E-05	1.42618	0.0013	960.28	20.15	899.95	38.59	1002.0	38.9	-6.7	4.2	960.28	20.15
G29	42	243	0.4957	0.16409	0.0007	1.56781	0.0065	979.47	26.90	957.56	28.87	997.5	27.3	-2.3	1.8	979.47	26.90
G12	30	169	0.4032	0.17181	0.0002	1.61293	0.0026	1022.08	20.91	975.25	37.14	1005.6	37.0	-4.8	-1.6	1005.6	37.0
G99	159	853	0.30	0.1844	0.0001	1.8227	0.0017	1090.7	4.3	1053.7	25.1	1045.8	24.8	-3.5	-4.3	1090.7	4.3
G19	32	149	0.7721	0.18905	0.0005	1.90018	0.0104	1116.23	24.57	1081.15	42.97	1094.3	42.5	-3.2	-2.0	1094.3	42.5
G96	464	1560	0.07	0.3051	0.0113	4.5378	11.2816	1716.4	115.2	1737.9	282.1	1805.0	277.8	1.2	4.9	1805.0	277.8
G76	432	1300	0.44	0.3114	0.0033	4.6589	0.0961	1747.4	35.9	1759.9	29.7	1825.1	22.9	0.7	4.3	1825.1	22.9
G71	297	1020	0.26	0.2872	0.0030	4.2845	0.0814	1627.4	33.3	1690.4	27.7	1834.4	21.0	3.7	11.3	1834.4	21.0
G72	259	732	0.28	0.3396	0.0036	4.9411	0.1024	1884.8	38.1	1809.3	29.7	1840.0	22.3	-4.2	-2.4	1840.0	22.3
G75	451	1271	0.34	0.3376	0.0035	5.2875	0.0974	1874.9	37.0	1866.8	28.2	1841.6	20.8	-0.4	-1.8	1841.6	20.8
G40	124	391	0.4315	0.29899	0.0001	4.54588	0.0027	1686.30	20.55	1739.41	59.53	1847.1	60.2	3.1	8.7	1847.1	60.2
G100	27	63	0.62	0.3709	9E-05	5.0831	0.0103	2033.8	20.1	1833.3	139.2	1847.7	137.2	-10.9	-10.1	1847.7	137.2
G66	258	736	0.33	0.3341	0.0035	4.9296	0.0952	1858.2	37.0	1807.3	28.0	1849.0	20.4	-2.8	-0.5	1849.0	20.4
G48	248	771	0.2866	0.31284	0.0012	4.84016	0.015	1754.67	30.75	1791.91	29.33	1864.3	27.2	2.1	5.9	1864.3	27.2

G15	166	539	0.1613	0.30922	0.0028	4.94358	0.0712	1736.87	46.34	1809.73	39.19	1865.6	32.6	4.0	6.9	1865.56	32.58
G28	169	531	0.2960	0.30965	0.0006	4.84085	0.0049	1738.98	24.77	1792.03	26.03	1871.4	25.4	3.0	7.1	1871.4	25.4
G2	161	498	0.4631	0.30129	0.0008	4.65187	0.01	1697.70	27.39	1758.63	27.28	1874.4	26.0	3.5	9.4	1874.4	26.0
G77	189	557	0.31	0.3263	0.0036	4.6627	0.1039	1820.4	37.9	1760.6	31.8	1880.5	25.0	-3.4	3.2	1880.5	25.0
G54	215	701	0.1017	0.31277	0.0025	4.89606	0.092	1754.32	43.72	1801.58	39.04	1889.4	33.9	2.6	7.1	1889.4	33.9
G59	229	585	0.76	0.3394	0.0037	4.9440	0.1136	1883.7	39.1	1809.8	31.0	1892.1	23.6	-4.1	0.4	1892.1	23.6
G102	118	369	0.417	0.30211	0.0005	4.74221	0.0052	1701.8	24.2	1774.7	26.8	1892.4	26.4	4.1	10.1	1892.4	26.4
G68	208	603	0.23	0.3360	0.0036	4.9105	0.1063	1867.6	38.3	1804.1	30.2	1897.9	22.9	-3.5	1.6	1897.9	22.9
G97	111	334	0.32	0.3200	0.0034	4.6586	0.1057	1789.5	36.5	1759.8	33.5	1997.9	27.9	-1.7	10.4	1997.9	27.9
G35	172	365	0.4934	0.4249	0.0006	8.53751	0.0087	2282.69	24.51	2289.92	27.51	2323.6	27.1	0.3	1.8	2323.6	27.1
G82	412	928	0.32	0.4194	0.0044	8.5271	0.1681	2257.6	43.5	2288.8	32.0	2374.7	24.7	1.4	4.9	2374.7	24.7
G23	207	407	0.3716	0.46735	0.0009	10.9063	0.0128	2471.93	27.52	2515.17	26.00	2551.3	24.9	1.7	3.1	2551.3	24.9
G69	921	1675	0.08	0.5231	0.0054	13.3427	0.2323	2712.4	48.4	2704.2	28.9	2698.7	20.2	-0.3	-0.5	2698.7	20.2

Table 3. Values of *p* obtained from K-S tests comparing U-Pb zircon age spectra among sediment samples.
Values are rounded and reported to three significant figures. Bold indicates $p<0.05$, representing samples that (at 95% confidence) do not come from the same population.

	Thar Chak-310	Thar UN1	Thar NM3	Sutlej River	Nara	Indus River, modern	Indus 7 ka TH-10	Indus LGM KB-41-5
Thar Chak-310		**0.027**	**0.029**	**0.000**	**0.000**	0.352	**0.000**	**0.000**
Thar UN1	**0.027**		**0.024**	**0.000**	0.326	**0.001**	0.265	0.267
Thar NM3	**0.029**	**0.024**		**0.000**	**0.009**	**0.041**	**0.001**	**0.001**
Sutlej River	**0.000**	**0.000**	**0.000**		**0.000**	**0.000**	**0.000**	**0.000**
Nara	**0.000**	0.326	**0.009**	**0.000**		**0.000**	0.400	0.926
Indus River, modern	0.352	**0.001**	**0.041**	**0.000**	**0.000**		**0.000**	**0.000**
Indus 7 ka TH-10	**0.000**	0.265	**0.001**	**0.000**	0.400	**0.000**		0.204
Indus LGM KB-41-5	**0.000**	0.267	**0.001**	**0.000**	0.926	**0.000**	0.204	

Table 4. New Nd isotopic analyses from the southern Punjabi floodplain region of the Sutlej and Ghaggar-Hakra river courses. Sample S4-081109-18 is aeolian sediment, all others are fluvial.

Sample	Location Name	Latitude	Longitude	Depth subsurface (m)	$^{143}Nd/^{144}Nd$	Error (2σ)	εNd
S3-Sutlej River 20-63μm	Tatapani	31°14'41.15"N	77° 5'24.21"E	0	0.511660	8.00E-06	**-19.07**
S9-CJ-4-1 91-103 cm	Alkasur Cotton Jinner	29° 9'5.32"N	71°51'19.46"E	0.97	0.511886	1.28E-05	**-14.68**
S6-CJ-4-7, 233-240 cm, 20-63 μm	Alkasur Cotton Jinner	29° 9'5.32"N	71°51'19.46"E	2.37	0.511854	9.00E-06	**-15.29**
S10 CJ-4-10, 291-300 cm	Alkasur Cotton Jinner	29° 9'5.32"N	71°51'19.46"E	2.96	0.511897	1.20E-05	**-14.45**
S19 M1 0.27-0.30	Marot	29°12'47.76"N	72°20'28.38"E	0.29	0.511881	1.76E-05	**-14.76**
S20 M2A 1.93-1.95	Marot	29°12'47.76"N	72°20'28.38"E	1.94	0.511935	1.24E-05	**-13.72**
S13 M2A 2.59-2.64	Marot	29°12'47.76"N	72°20'28.38"E	2.61	0.511924	1.32E-05	**-13.92**
S14 M2B 3.0-3.02	Marot	29°12'47.76"N	72°20'28.38"E	3.01	0.511925	9.80E-06	**-13.91**
S15 M5A 8.95-8.97	Marot	29°12'47.76"N	72°20'28.38"E	8.96	0.511865	6.80E-06	**-15.07**
S16 M12A 29.88-29.90	Marot	29°12'47.76"N	72°20'28.38"E	29.89	0.511847	7.60E-06	**-15.42**
S17 T2 3.42-3.45	Tilwalla	29° 5'42.22"N	71°34'3.39"E	3.44	0.511878	7.00E-06	**-14.83**
S18 T4 9.18-9.20	Tilwalla	29° 5'42.22"N	71°34'3.39"E	9.19	0.511823	4.00E-06	**-15.90**
S4-081109-18, <63 μm	Yazman (aeolian)	29° 7'23.16"N	71°46'10.08"E	0	0.511895	9.20E-06	**-14.50**
S8-081109-17, 20-63 μm	Yazman	29° 7'23.16"N	71°46'10.08"E	0.70	0.511880	1.46E-05	**-14.79**
S1-081109-16, 20-63 μm	Yazman	29° 7'23.16"N	71°46'10.08"E	1.50	0.511887	9.60E-06	**-14.65**
S5-081109-15, 20-63 μm	Yazman	29° 7'23.16"N	71°46'10.08"E	2.30	0.511881	1.20E-05	**-14.78**
S7-081109-14, 20-63 μm	Yazman	29° 7'23.16"N	71°46'10.08"E	2.90	0.511891	8.40E-06	**-14.56**
S11 081109-11, 20-63 μm	Yazman	29° 7'23.16"N	71°46'10.08"E	3.70	0.511880	1.04E-05	**-14.79**

Table 5. Percentages of different age groups in U-Pb zircon age spectra for Indus River end-member sediment sources from three time periods (LGM, 7 ka, and modern) considered in mixing calculations, together with relative abundance in three Thar Desert dune sand samples from which zircon data are available (NM3, UN1, and Chak-310). Also shown are Nd isotope compositions for the end members.

Age groups (Ma)	Indus LGM	Indus 7 ka	Indus modern	Sutlej River	NM3	UN1	Chak 310
0-300	46.9	48.6	23.5	3.0	43	40	22
300-750	23.2	17.7	17.6	10.1	14	24	26
750-1250	19.5	20.0	22.4	27.3	16	18	23
1500-2300	10.4	13.7	36.5	59.6	28	19	29
ε_{Nd}	-10.8	-13.5	-15.3	-19.0			